Magnetic fingerprint of southern Portuguese speleothems and implications for paleo- and environmental magnetism

Eric Font[1*], Cristina Veiga-Pires[2], Manuel Pozo[3], Claire Carvallo[4], António Carlos de Siqueira Neto[5], Pierre Camps[6], Sébastien Fabre[7] and José Mirão[8].

[1] *IDL-FCUL, Instituto Dom Luís, Faculdade de Ciências, Universidade de Lisboa, Portugal*
[2] *CIMA-FCT, Universidade do Algarve, Campus de Gambelas, 8005-139 Faro, Portugal*
[3] *Departamento de Geología y Geoquímica, Universidad Autónoma de Madrid, 28049-Madrid, Spain*
[4] *Institut de Minéralogie, de Physique des Minéraux et de Cosmochimie, Sorbonne Universités - UPMC Univ Paris 06, UMR CNRS 7590, Muséum National d'Histoire Naturelle, IRD UMR 206, 4 Place Jussieu, F-75005 Paris, France*
[5] *IAG-USP, Universidade de São Paulo, Brazil*
[6] *Géosciences Montpellier, CNRS, Université Montpellier 2, Montpellier, France*
[7] *IRAP, Université de Toulouse, France*
[8] *HERCULES, Evora, Portugal*

***Corresponding author:** Eric Font, IDL-FCUL, Instituo Dom Luiz, Universidade de Lisboa, Edifício C8-8.3.22, Campo Grande, 1749-016, Lisboa, PORTUGAL. Phone: +351 217500811; e-mail: font_eric@hotmail.com

This article has been accepted for publication and undergone full peer review but has not been through the copyediting, typesetting, pagination and proofreading process which may lead to differences between this version and the Version of Record. Please cite this article as doi: 10.1002/2014JB011381

Abstract

Environmental magnetism of speleothems is still in its early stage of development. Here we report on our investigation of the environmental and paleomagnetic information that has been recorded in speleothems, and what are the factors that control its preservation and reliability. To address these issues, we used a multidisciplinary approach, including rock magnetism, petrography, scanning electron microscopy, stable carbon and oxygen isotope compositions, and major and trace element concentrations. We applied this to a set of samples from different stages of speleothem evolution: present-day dripwater (glass plates), a weathered stalactite, a fresh stalagmite, cave sediments and terra rossa soils. These samples come from the Penico and Excentricas caves, located in two distinct aquifers of the Algarve region, South Portugal. Our results show that the main magnetic carriers of the speleothems under study are primary (detrital) and consist of maghemite (and magnetite?). Similarities in coercivity- and temperature-dependence of the studied set of samples suggest that iron oxides are inherited from the terra rossa soils that cap the cave and were transported to the speleothems by dripwater. Hence, they represent a regional environmental signature. Interestingly, a stable, and probably detrital remanent magnetization could be isolated in the fresh stalagmite, whereas the weathered stalactite yielded chaotic magnetic directions and very low remanent intensities. We propose that these low intensities can be the result from: i) different remanence acquisition mechanisms between stalagmite and stalactite and/or ii) iron dissolution by fungal activity. We also suggest that magnetic properties, color and the content in detrital elements in the fresh speleothem inform about environmental processes acting on the interface of rock (soil)-atmosphere, while oxygen isotope composition and alkaline-earth element concentrations inform about calcite-water interaction processes. These results provide a better understanding of how environmental information is recorded in speleothems and what the factors are that control the reliability of the paleomagnetic and paleoenvironmental signal.

Keywords: speleothem, magnetism, environment, SEM, fungi, Portugal.

1. Introduction

Paleo- and environmental magnetism of speleothems is likely to be of increasing interest in the near future [*Lascu and Feinberg*, 2011; *Liu et al.*, 2012; *Osete et al.*, 2012]. Speleothems are excellent recorders of Quaternary climate and environmental changes. When underpinned by precise and accurate radiometric dating, the isotopic, geochemical and mineralogical signatures preserved in the thin laminations provide high-resolution climate-proxy time series, from sub-annual (i.e. seasonal) to millennial scales. Speleothems have been reported to host magnetic minerals in readily measurable concentrations using standard rock magnetic techniques. Magnetic direction conforming to those of the ambient Earth´s magnetic field (at the time of deposition) are preserved through a mechanism called detrital remanent magnetization (DRM) in possible combinations with a chemical remanent magnetization (CRM), acquired by in-situ precipitation of iron oxides. For a comprehensive review of the magnetism of speleothems, the reader is directed to Lascu and Feinberg (2011). Implicitly, magnetic studies of speleothems contribute information about two important areas of geosciences. First, speleothems can provide high-resolution records of short-term variations of the ancient geomagnetic field, or their converse, that allow the use of paleomagnetism as a dating tool of speleothems [*Lascu and Feinberg*, 2011; *Latham et al.*, 1979; *Lean et al.*, 1995; *Morinaga et al.*, 1992; *Openshaw et al.*, 1997; *Osete et al.*, 2012; *Pruner et al.*, 2010; *Stock et al.*, 2005; *Strauss et al.*, 2013]. Second, speleothems can provide a record of climate variability by linking rock magnetic properties to changes in detrital input driven by regional and global climate and environmental forcing parameters [*Ellwood and Gose*, 2006]. A prerequisite to ensuring the reliability of paleo- and rock magnetic data from speleothems, either as a dating tool or as an environmental parameter, is to demonstrate that the magnetic mineralogy is "primary" (i.e. the remanence acquisition was contemporaneous to deposition time) and has subsequently been preserved. A good understanding of the nature, origin and concentration of magnetic minerals preserved in speleothems and their link with the composition of the detrital supply and possible source areas is therefore essential. However, in a number of well documented speleothem studies, recording short-term geomagnetic field variations [e.g. *Osete et al.*, 2012; *Pruner et al.*, 2010], little attention has yet been given to their magnetic mineralogy. For example, the processes by which environmental information recorded in speleothems is still poorly constrained. This is so, even when stable isotope and rock magnetic data are included, as well as the effects of post-depositional alterations such as microbial activity on the reliability of the environmental and paleomagnetic signal. In this

study we address these issues by studying a set of samples from two caves from the Algarve region in southern Portugal, the Penico and Excentricas caves (Fig. 1). Their deposits cover different stages of speleothem evolution, including: i) glass plates positioned underneath drip sites (from January to March 2012); ii) a stalactite with visible alteration features, such as moon-milk from the Penico cave, and iii) a fresh stalagmite from anotheraquifer (Excentricas cave). In order to compare the magnetic mineralogy of the fresh speleothem with the surrounding detrital sources, we studied cave sediments inside the Excentricas cave and terra rossa soils lying above the cave.

We first checked the composition and alteration processes using petrographic and scanning electron microscopy (SEM) analysis. We measured carbon and oxygen isotopic ratios in order to identify eventual diagenetic alterations. We analyzed iron phases by using SEM and rock magnetic techniques, such as thermomagnetic analysis, isothermal and anhysteretic remanence acquisition, hysteresis and First-Order Reversal Curve (FORC) diagrams. We then measured paleomagnetic directions of the speleothem samples in order to evaluate whether the paleomagnetic signal is preserved in the weathered stalactite. In the case of the fresh stalagmite, where stable natural remanent magnetization (NRM) directions were recorded, we conducted major and trace element analyses (X-ray fluorescence and inductively-coupled plasma mass spectrometry, ICPMS), as well as visible diffuse reflectance spectrophotometry. Lastly, we discuss the influence of microbial activity on the remanence intensities, and describe how magnetic properties, color, stable isotope composition and mineralogy can provide information about the speleothems and the environment in which they formed.

2. Materials

We selected one speleothem from each of two caves located in the Algarve Basin of southern Portugal (Fig. 1A). A fresh stalagmite (SPAII; Fig. 1B) was collected in situ in the Excentricas cave, located in the karstic aquifer of Peral-Moncarapacho (area of 44 km^2). A weathered speleothem (SPA) fragment, which corresponds to a broken piece of stalactite collected from the ground, was taken from the Penico cave (aquifer of Querença-Silves, 318 km^2). Both aquifers are essentially developed in Jurassic carbonates and are separated by ~40 km (Fig. 1A). Weathering in the SPA stalactite is visible at the naked eye by the presence of moon-milk, a disintegration product of calcite that is generally interpreted to result from microbial activity (Fig. 1C,D) [*Barton and Northup,* 2007*; Braissant et al.,* 2012*; Cañaveras*

et al., 2006*; Cañaveras et al.,* 1999]. We also collected cave sediments (samples SG1) and terra rossa soils, developed on Jurassic limestones and located above the Excentricas cave (samples TR1, TR2 and TR3; Fig. 1A).

Watch (convex up) glasses with a diameter of 7 cm were positioned underneath the drip sites of the Penico cave, where the weathered stalactite was found. These glass plates remained in the cave during three months, from January through March 2012. The convex side up shape of the glass plate was chosen to mimic the shape of a stalagmite tip and to avoid water accumulation and stagnation [*Daeron et al.,* 2011; *Riechelmann et al.,* 2013].

3. Sampling and methods

For paleomagnetic analysis, the SPA (samples SPA_6 and SPA_10) and SPAII (SPAII_1 and SPAII_2) speleothems were cut into individual specimens of 2x2x2 cm (standard size of the JR6 magnetometer) by using a non-magnetic Dremel-saw. We referenced the magnetic directions relative to the vertical axis of the front side of the cubic samples because speleothems were not oriented in the field. In addition, we collected thin calcite growth laminae and filled them into standard 2x2x2 cm plastic boxes (samples SPAII_4 to SPAII_12) for subsequent bulk magnetic property measurements. Cave sediments and terra rossa were crushed by using an agate mortar for subsequent thermomagnetic analysis.

Rock-magnetic measurements were performed in the Paleomagnetism Laboratory of the Instituto Dom Luís (IDL) of Lisbon, Portugal. Remanence was measured by using a JR6 magnetometer (sensitivity of 2.4×10^{-6} A/m). Demagnetization treatment included stepwise alternating field (AF) up to 100 mT. The measurements were subject to Principal Component Analysis (PCA) of the NRM. We also measured bulk magnetic properties by using concentration and coercivity dependent proxies. Magnetic susceptibility (MS) was measured with a MFK1 (AGICO) apparatus and reported relative to mass (m^3/kg). Low and high temperature dependence of MS were conducted under Argon-controlled atmosphere. Minimizing the influence of magnetic interactions [*Heslop et al.* [2004] by limiting the AF steps to 100mT, samples were subsequently submitted to isothermal remanent magnetization (IRM) acquisition with an impulse magnetizer (model IM-10-30). We applied maximum fields of 1.2T following approximately 25 steps. Data were analyzed using a cumulative log-Gaussian (CLG) function [*Robertson and France,* 1994] with the software developed by *Kruiver et al.* [2001]. The S-ratio was calculated with the formula $-IRM_{-0.3T}/IRM_{1T.}$ For the

modified Lowrie-Fuller test [*Johnson et al.*, 1975], anhysteretic remanent magnetization (ARM) was induced by a combination of an AF field of 100mT and a DC field of 0.05mT using a LDA-3A demagnetizer coupled to an AMU-1A anhysteretic magnetizer (AGICO).

Hysteresis curves and FORC diagrams were measured using a magnetometer (µ-VSM) from Princeton Measurements Corporation within the IPGP-IMPMC Mineral Magnetism Analytical Facility. Since the magnetization of speleothems is very weak, each sample was crushed into a powder and tightly packed in a gelcap, in order to maximize the amount of material for the measurement, instead of using only a millimetric chip as it is usually done with the µ-VSM. Data are treated using the FORCInel software [*Harrison and Feinberg*, 2008].

Fresh rock fragments as well as glass plates were observed under a Hitachi S-3700N SEM microscope coupled to a Bruker XFlash® 5010 EDS detector at the Hercules laboratory (Évora, Portugal). The electron source for the SEM is a tungsten wire. The accelerate voltage is 20 keV. Qualitative compositional analysis is provided by energy dispersive spectra (EDS) by using the ESPRIT Software (Bruker).We also conducted Diffuse Reflectance Spectrophotometry (DRS) analysis, which is based on the percentage reflectance of a sample relative to white light and provides qualitative information about mineralogical variations. DRS data were represented in the CIE (1978) L*a*b* space where L* is the black/white reflectance, a* is the redness/greenness and b* is the yellowness-blueness. Data were obtained using a X-Rite® Colortron™ spectrophotometer from rock powders (in order to avoid grain size effect) using the mean value of three series of measurements.

Contents in major elements, trace elements and loss on ignition (LOI) of 12 samples collected from the SPAII speleothem have been analyzed at the Geological Survey of Spain (IGME). The chemical analysis of Si, Al, Mg, Fe, K, Mn, Ti, P and Ca was performed by means of the MagiX X-ray fluorescence (XRF) spectrometer of PANalytical. Samples were analyzed after glass disc elaboration from molten mixture of sample with lithium tetraborate. The values of major elements are expressed as oxides weight percentage (%wt). Lost on ignition was determined at 950ºC. Trace element concentrations were determined by inductively coupled plasma spectrometry in both ICP-OES (OE=optical emission; As, Ba, Be, Co, Cr, Cu, Ni, Sr, V, Zn, Pb) and ICP-MS (Th, U) analytical instruments. Samples were analyzed in standard procedures by acid digestion (FH, HNO_3 and $HClO_3$). The values of trace elements are expressed in ppm.

C and O isotopic analysis of 13 samples were performed at the laboratories of the Interdepartmental Research Service (SIDI) of the Universidad Autónoma de Madrid. Carbon dioxide was evolved from each sample at 25 ºC using 100% H_3PO_4. All samples were prepared and analyzed at least in duplicate. The analytical precision is generally ± 0.10‰ for carbon and ± 0.15‰ for oxygen. Both oxygen and carbon isotopic ratios are reported in δ and expressed in permil relative to Vienna Pee Dee Belemnite (VPDB).

4. Petrographic and Scanning Electron Microscopy

Glass plates (Penico cave)

The convex up glass plates collected underneath the drip sites of the Penico cave (where the weathered stalactite was collected) revealed widespread microfungal activity in close relation to calcite crystals (Fig. 2A-D). These fungi have been identified by rRNA (ribosomal ribonucleic acid) sequenciation and correspond to the genus *Mortierella* (Fonseca, F., *pers. comm.*), from the order of *Actinomycetales*. This organism is known to develop in soils and organic material but it has also been described as occurring in caves [*Cañaveras et al.*, 1999; *Degawa and Gams*, 2004; *Vaughan et al.*, 2011]. An isolated spherical cell of more than 100 μm wide (flattened on the photograph due to vacuum; Fig. 2D) was also observed and assigned to be a sporangiospore produced by *Mortierella* [*Wang et al.*, 2011]. From a mineralogical point of view, calcite crystals have an average size of the order of 100μm and exhibit sub-euhedral and rounded shapes (Fig. 2C). Furthermore, crystals observed in an area where fungi are not present have euhedral shape suggesting that microorganisms are responsible for the calcite consumption/dissolution. Such interpretation is reinforced by Figure 2C in which calcite crystals seem to serve as an anchor for the development of the fungal hyphal tips and networks. Fungi penetrating a mineral grain have also been described in other environments such as soils [figure 3 in *van Scholl et al.*, 2008].

In addition to fungi, rare Ti-bearing iron oxides were observed (Fig. 2E). A high ratio of Ti:Fe shown by EDS (Fig. 2E) suggests an Fe-bearing Ti-oxide (ilmenite or pseudo-brookite). The size (~5μm) and eroded borders of the crystal suggest a detrital origin. Detrital input is also evidenced by the presence of an isolated crystal of zoned zircon (Fig. 2F).

The presence of zircon as well as the Ti-oxide argues for a detrital contribution of the magnetic carriers transported by present-day drip-waters in the Penico cave and suggests that magnetic iron oxides should have been originally present in the weathered stalactite under

study. The widespread development of fungi observed in the Penico cave make the SPA stalactite an excellent target to study the relation between iron oxide preservation and microbial activity.

Weathered stalactite (Penico cave)

Moon-milk of the weathered stalactite was observed under optical and electron microscope in thin sections and rock fragments, respectively (Fig. 3). A detailed search for iron oxides was unproductive due to the very low content of iron oxides. Under optical microscope, rare opaque minerals are found filling intergranular spaces (Fig. 3A) or as isolated crystals showing halo of iron oxidation (Fig. 3B). Under SEM, Ti-free iron compounds are represented by very fine (~3 μm in length) severely oxidized aggregates of iron oxides (Fig. 3C) and very fine (<5 μm) Fe-Ti iron oxides associated to detrital material (Al and Si on EDS spectra) (Fig. 3D-E). Spheroidal concretions of unknown composition, due to the very small size, are locally observed (Fig. 3F) and are similar to biogenic concretions observed in other speleothems (see fig. 3 in *Cañaveras et al.* [1999]) or to cosmic spherules [*Strauss et al.*, 2013].

Optical petrographic observations of the calcite fabrics reveal widespread recrystallization processes that disrupt the original calcite lamination (Fig. 3G-H). Under SEM microscope, these altered areas are consisting of spiky calcite (a destructive fabric formed by etching) and microcrystalline calcite partially associated to biocrystalline assemblages constituted of anhedral calcite crystals and needle-fiber calcite (Fig. 3I-L). Spiky calcite and needle-fiber calcite are common in moon-milk deposits and are generally interpreted to result from microbial activity [*Barton and Northup*, 2007; *Braissant et al.*, 2012; *Canaveras et al.*, 2006; *Cañaveras et al.*, 2001; *Cañaveras et al.*, 1999].

Fresh stalagmite (SPAII, Excentricas cave)

SEM-EDS analyses were conducted on specimen SPAII_7 that is composed of white and pink-brown laminations. A difference in the crystallography of the calcite layers is noted (Fig. 4A-C): A thin (~1μm) level composed by columnar calcite (~20μm wide) is oriented normal to the stratification plane. Columnar calcite is a common growth texture in stalagmites that grow in continuously wet environments from fluids at near-equilibrium

conditions [*Frisia et al.*, 2000]. Multiple voids are ubiquitous on the surface of calcite crystals (Fig. 4D). Iron oxides were easily observable and essentially represented by small crystals of Ti-bearing iron oxides (Fig. 4E-G). Darker zones of the crystal correspond to higher titanium contents relative to iron (Fig. 4E). Morphologies are either cubic or semi-hexagonal with grain size up to some ten of micrometers (<20μm). The eroded aspects of the crystals together with the presence of titanium demonstrates the terrigenous and detrital origin of the main magnetic carriers of the preserved stalagmite.

Based on SEM observations and EDS analyses, we suggest that detrital grains are identical between the two caves under study.

5. C and O isotopes

Carbon and oxygen isotope ratios were determined in five specimens from the weathered stalactite and eight specimens from the fresh stalagmite. Results are illustrated in Figure 5A and Table 1 and compared with the oxygen and carbon stable-isotope values of active fabrics (recently deposited calcite) from the Grotta del Calgeron (Alpes) and Crag Cave (Ireland) [*Frisia et al.*, 2000]. The studied Portuguese speleothems show consistent stable isotope compositions within the sample collection (Fig. 5A, Table 1). Samples from the fresh stalagmite exhibit very narrow $\delta^{13}C$ values close to -8.5 ‰, while the weathered stalactite show more scattered $\delta^{13}C$ values varying from -2.9 to -5.7 ‰. The same is observed for $\delta^{18}O$ values that range from -1.5 to -2.8 ‰ and -1.7 to -2.4‰ in the weathered and fresh speleothem, respectively. Such differences in stable isotope composition of the two speleothems (two neighbor caves) under study may reflect post-depositional calcite alteration and/or differences in calcite crystallinity and texture (dendritic, columnar, microcrystalline, fibrous) such as was also observed in the case of the Crag Cave and the Grotta del Calgeron [*Frisia et al.*, 2000].

Variations in speleothem $\delta^{18}O$ values generally result from the interplay of complicated natural processes in the ocean, atmosphere, soil zone, epikarst, and cave system, making the interpretation of $\delta^{18}O$ data extremely complex [*Lachniet*, 2009]. Despite uncertainties in $\delta^{18}O$ climate calibrations linked to regional and local factors (mean annual air temperature, precipitation, altitude, continentality and humidity that can vary in space and time), $\delta^{18}O$ time series in speleothems provide unprecedented insight into environmental and climate studies. A recent compilation of $\delta^{18}O$ composition from European speleothems show a striking spatial

distribution of the data as a function of longitude, interpreted to reflect the influence of the Atlantic moisture and continentality [*McDermott et al.*, 2011] (Fig. 5B). These isotopes gradients can be used to recognize anomalous $\delta^{18}O$ values in speleothems that could reflect local site-specific effects and/or systematic seasonal biases. When compared to the present-day European $\delta^{18}O_{speleothems}$ compilation from *McDermott et al.* [2011], $\delta^{18}O$ values of the Portuguese speleothems are close to the values expected for their corresponding longitude (~8ºW at Faro) (Fig. 5B), confirming the primary nature of the isotopic signal. The same interpretation is valid for the active fabrics of the Italian (Grotta di Ernesto and Grotta del Calgeron) and Irish (Crag Cave) caves studied by *Frisia et al.* [2000], which also show $\delta^{18}O$ composition in agreement with their longitude (Fig. 5B). However, slightly but significantly lower $\delta^{18}O$ values of the Portuguese speleothems, compared to the Irish Crag results, may be linked to peculiar regional climatic conditions, because the Algarve region may have been influenced by Atlantic as well as Mediterranean climatic conditions.

These results indicate that the oxygen isotopic composition of the speleothems under study is primary and has been preserved until now. Oxygen isotopic compositions of the weathered and fresh stalagmite can thus be used as a robust climatic and environmental proxy for southern Portuguese speleothems.

6. Magnetic Mineralogy

6.1. Thermomagnetic (χ-T) analysis

Identification of the nature and composition of ferromagnetic (sensus lato) minerals can be first investigated through the determination of their Curie temperatures from the analysis of thermomagnetic curves (χ vs. T). Out of twelve studied speleothem samples, only four (corresponding to brown-red laminations where higher IRM-NRM values were measured) gave reliable measurements, whereas the other samples presented very low χ values below the resolution of the equipment. We also conducted thermomagnetic analyses on terra rossa soils from three sites around the area of the Excentricas cave (SPAII), as well as from cave sediments. Figure 6 shows thermomagnetic curves of characteristic samples after normalization by mass and after subtracting holder values. All samples show a hump at around 200-300ºC characteristic of maghemite and another one at around 460-500ºC with a Curie temperature of 550-580ºC typical of magnetite (Fig 6-A-F). In the terra rossa and cave sediment samples, the hump at 250-300ºC is much more pronounced, probably due to higher

content of magnetic particles compared to the speleothems (Fig. 6-D-F). After heating up to 700ºC, neoformation of magnetite is observed in all cooling cycles (Fig. 6). The newly formed magnetite has Curie temperatures comparable to those observed in the heating cycles and remains stable even after two successive heating cycles up to 700ºC (Fig. 6-G).

The accurate determination of the nature of the original magnetic carriers through thermomagnetic analysis is not straightforward in this case, since important mineralogical transformations occur during the heating process. For example, the shapes of thermomagnetic curves are quite similar to those obtained from air/temperature oxidation of siderite, which typically produces maghemite, magnetite and hematite as transformation products [*Pan et al.*, 2000]. However, reversibility in heating and cooling curves in the case of siderite occurs at around 300ºC, while stepwise thermal heating/cooling cycles indicate that irreversibility (i.e. formation of new magnetic phases) occurs between 400-450ºC (Fig. 6-H). Moreover, siderite is rare in cave systems [*Hill and Forti*, 1997] and has thus far not been identified by X-ray diffraction or SEM analysis (see below). We thus exclude siderite as potential host for the magnetic phases identified in heating cycles.

Detrital (pedogenic) maghemite and magnetite contained in soils and deposited in the calcite growth by drip-water are possible candidates. For example, thermomagnetic curves from paddy soil horizons from China and their corresponding dryland soils show the same pattern as those of the speleothems, soils and cave sediments under study [*Lu et al.*, 2012]. These authors explain the increase in magnetic susceptibility (MS) values up to ~250ºC by the conversion of poorly crystallized ferric oxides, such as ferrihydrite to maghemite, or magnetite in the presence of soil organic matter [*Hanesch et al.*, 2006; *Lu et al.*, 2012]. However, ferrihydrite is superparamagnetic at room temperature [*Cornell and Schwertmann*, 2003] and thus cannot be the magnetic carrier of the remanence measured during non-destructive magnetic analyses (AF demagnetization and IRM). Another possible explanation of the hump at 250ºC is the conversion of antiferromagnetic pyrrhotite (Fe_9S_{10}) to ferromagnetic pyrrhotite (Fe_7S_8) by heating [*Dunlop and Özdemir*, 1997]. However, pyrrhotite is metastable and its occurrence in oxidized soils such as terra rossa is unlikely. We rather interpret the MS increase up to 250ºC as a gradual passing of the SD/SP threshold, as an analog of a very wide Hopkinson peak, and the subsequent χ decrease up to 400ºC would then represent the transformation of maghemite into hematite. Maghemite has been ubiquitously described in terra rossa soils worldwide [*Bellanca et al.*, 1996; *Meert et al.*, 2009] and inverts to hematite between 200ºC and 380ºC [*Doubrovine and Tarduno*, 2006;

Dunlop and Özdemir, 1997; *Krása and Matzka*, 2007; *Özdemir*, 1987]. During stepwise progressive heating/cooling cycles of the SPAII_12 speleothem sample, heating and cooling curves are almost reversible until ~400ºC, but maximum χ values decrease progressively with successive heating/cooling cycles (at 200-250-300-350-400ºC), indicating that maghemite is being inverted to hematite (Fig. 6-H). Production of new magnetite occurs thereafter between 400 and 450ºC as shown by the irreversibility of heating and cooling curves and a Curie temperature close to 550-580ºC. Conversely, the magnetite with a Curie temperature of 550-580ºC observed in both heating and cooling cycles is probably formed during heating by the transformation of iron-bearing clay minerals and/or maghemite. The presence of pedogenic magnetite cannot be dismissed, but its contribution relative to the magnetite formed during heating is not resolvable through thermomagnetic analysis.

Regardless of the exact composition of the ferromagnetic phases, a strong similarity in the shapes of warming and cooling curves between the speleothems (Fig. 6-A-C), terra rossa (Fig. 6-D-E) and cave sediments (Fig. 6-F) indicates that iron-bearing phases in these samples are identical. Such a similarity in magnetic phases between the caves of different aquifers and country rocks (terra rossa) suggests that the magnetic mineral assemblage of speleothems is of detrital nature and reflects the composition of the source rocks.

6.2. Isothermal Remanent Magnetization analysis

Isothermal Remanent Magnetization (IRM) was induced in 7 specimens from SPA and 15 specimens from SPAII (Figs. 7-8). After treatment by the Cumulative Log-Gaussian function [*Kruiver et al.*, 2001; *Robertson and France*, 1994], best fits of the raw IRM curves are obtained by considering three components (Figs. 7-8, Table 2). Results between the fresh and the weathered speleothems differ in the relative proportion of each component.

The fresh stalagmite SPAII yields homogeneous and reproducible results independently of the color of the lamination (except for concentration-dependent magnetic proxies such as the saturation isothermal remanent magnetization, SIRM). All specimens are systematically characterized by a tri-modal association of coercivity spectra, namely a low coercive phase (comp. 1), thought to be magnetite/maghemite ($B_{1/2}$~23 mT), and two higher coercive phases (comp. 2 and 3) with mean $B_{1/2}$ ~120 mT and 580 mT. These values are in the range of hematite and goethite respectively [*Abrajevitch and Kodama*, 2011] (Fig. 7; Table 2). Component 2 and 3 have very low remanence intensities, leading to noisy CLG fits (Fig. 7-

8). Therefore we have not considered their magnetic properties in our interpretation. Component 1 is dominant in all samples and contributes to more than 86% of the total remanence (Table 2). Mean acquisition fields (i.e. $B_{1/2}$~Hcr) and dispersion parameter (DP) values of component 1 are similar to those of magnetite contained in continental flood basalts (CFB) [*Font et al.*, 2011; E. Font, unpublished data] and speleothems [*Lascu and Feinberg*, 2011] (Fig. 7D-E). Maghemite, a by-product of magnetite oxidation already described in speleothems [*Brook et al.*, 2006; *Lascu and Feinberg*, 2011], also shares a comparable range of coercivity. DP shows very consistent values (0.20-0.30, Table 2) for all three components (Table 2) suggesting homogenous populations in term of grain size and composition [*Egli*, 2004], probably due to efficient sorting during transport along the hydrological pathway. Furthermore, component 1 shows a striking clustering of the $B_{1/2}$ values indicating strong compositional homogeneity of the magnetic carrier population (Fig. 7). The concentration of iron oxides, measured by the mass normalized SIRM values, is systematically higher in brown layers. These characteristics suggest that post-depositional oxidation has been minor in SPAII and did not significantly affect the original magnetic mineralogy (Fig. 4).

Similarly to SPAII, IRM data of the weathered stalactite SPA show three distinct magnetic phases (Fig. 8, Table 2). The lowest coercive phase (comp. 1) contributes from 54 to 94% of the total remanence. $B_{1/2}$ and DP values of component 1 are comparable to titanomagnetite from CFB (Fig. 8D-E), whereas component 2 and 3 are assigned to be hematite and goethite, respectively. Samples SPA3 and SPA9, which correspond to the reddish external rim of the stalactite, present IRM curves and cumulative log-gaussian (CLG) parameters very similar to the fresh SPAII stalagmite. However, all other samples affected by moon-milk recrystallization and influenced by widespread microbial activity show a drastic depletion in the relative contribution of component 1 in the total remanence (Fig. 8).

The similarity of thermomagnetic curves and CLG parameters of the external rim of the weathered stalactite (samples SPA_3 and SPA_9) and those of the fresh stalagmite indicates that the nature and origin of the magnetic carriers (magnetite/maghemite, hematite and goethite) are the same in the two studied caves (40 km apart). In addition, systematically lower SIRM values in the most weathered samples argue for the loss of iron oxides by post-depositional alteration (dissolution?).

6.3. The Lowrie-Fuller and Cisowski tests

The modified Lowrie-Fuller test [*Johnson et al.,* 1975] is based on the comparison of AF demagnetization curves of IRM and Anhysteretic Remanent Magnetization (ARM). The test was originally proposed to distinguish between single-domain (SD) and multi-domain (MD) magnetite grains, the ARM being harder to demagnetize than the IRM in SD grains. However, the reliability of the Lowrie-Fuller test has been challenged by contradictory results pointing out that the L-type (where ARM is harder to demagnetize than IRM, possibly being indicator of SD particles) and H-type (where IRM is harder to demagnetize than ARM, possibly being indicator of MD particles) may also be responses that are controlled by magnetic interactions between fine grained particles, the microcoercivity distribution, or a mixture of multicomponent grains [*Bailey and Dunlop,* 1983; *Egli,* 2004; *Egli and Lowrie,* 2002; *Halgedahl,* 1998; *Xu and Dunlop,* 1995]. However for a single population of low coercivity particles such as magnetite, the test remains a good first-order indicator of relative grain size and likely paleomagnetic stability. SPA samples yielded a range from L-type to mixed results (Fig. 9, Table 2) suggesting SD or a mixture of SD and MD domain states for the low coercive phase (i.e. magnetite/maghemite). The similarity of the IRM and ARM shapes within all samples argues for homogeneous populations in terms of grain size and microcoercivities as previously pointed out in IRM analysis by small variations in DP values of component 1 (see section 6.2.). Mixed results can also be interpreted as the admixture of slightly harder magnetic phases, such as maghemite or secondary magnetite with distinct grain sizes. All specimens from the SPAII stalagmite gave L-type responses in the test (Fig. 9, Table 2). Similarly, the reproducibility of the shape of IRM and ARM curves in all SPAII specimens corroborates IRM parameters obtained after CLG treatment (DP and $B_{1/2}$) and suggests the presence of a single and homogenous population of fine grained magnetite/maghemite as the principal magnetic carrier in the preserved stalagmite.

The *Cisowski* [1981] test helps to evaluate the degree of interaction of fine (SD) magnetic carriers. For the case of non-interacting SD particles the IRM acquisition and IRM demagnetization curves should be symmetrical. The point of intersection of the two curves is close to the remanent coercive force (Hcr) and its projection on the abscissa represents the degree of interaction, R. For all rock types, R values less than 0.5 indicate strong interaction of SD particles. However, it has been suggested that the R ratio is unable to differentiate between MD and interacting SD particles [*Fanjat et al.,* 2012]. The values of R and Hcr are very similar in all SPA and SPAII samples. R varies from 0.20 to 0.28 suggesting strong

interactions between SD (or MD?) particles (Fig. 9, Table 2). Hcr varies from 10 to 20 mT indicating a low coercive magnetic phase compatible with the presence of magnetite/maghemite. Note that both the modified Lowrie-Fuller and Cisowski tests are restricted to the identification of low to medium coercive phases such as magnetite, maghemite and pyrrhotite, due to limitation on the AF demagnetization field, which generally does not exceed 100 mT.

6.4. Hysteresis and FORC diagrams

Hysteresis curves and FORC diagrams [e.g. *Roberts et al.*, 2000] were determined in order to characterize the size of the magnetic carriers. Hysteresis loops were measured for every sample with an averaging time of 1 s. Most of the loops are dominated by diamagnetism, but once the diamagnetic contribution is removed, a small ferromagnetic contribution remains in some of the samples. Whenever this ferromagnetic contribution is not too small, we conducted FORC analysis with an averaging time between 3 and 4s and 80 reversal curves for one diagram (Fig. 10). Such an increase in the averaging time means that the measuring time is greatly increased, between 3 and 5 hours for one diagram, which also increases the risk of a possible drift in the loop measurement. The saturating field was set to 1T for all the FORC diagram measurements. The field step was set between 1.5 and 3.5 mT, depending on the H_u and H_c ranges that were chosen to obtain an optimized area for the most interesting features of the FORC diagrams. Hysteresis parameters are given in Table 2. M_{rs} values are on the order of 10^{-4}-10^{-5} Am^2/kg, which is very weak. Mr/Mrs values range between 0.007 and 0.14. Coercivity fields are very low (lower than 5mT), and Hcr/Hc values are between 2.46 and 5.42, with most values around 4-5. When plotted on a Day diagram with the mixing curves from *Dunlop* [2002], these hysteresis parameters fall between the SD-MD and the SD-SP mixing curves (Fig. 10A).

FORC diagrams were obtained for 6 samples from speleothem SPAII and 2 samples from speleothem SPA, which correspond to the more magnetized rim (SPA_3 and SPA_9; Table 2) of the stalactite. FORC diagrams were processed with the FORCInel software [Harrison and Feinberg, 2008] using the VARIFORC option [Egli, 2013]. With this option, larger smoothing factors are applied to the background, while preserving the areas along the axes with relatively small smoothing factors. The minimum smoothing factors on both axis were set to 3 and increased by steps of 0.1. Nevertheless, and despite the very long averaging time,

the FORC diagrams still contain a substantial amount of noise (Fig. 10B). Samples SPAII-11 and SPAII-12 (not shown in Figure 10) are characterized by a single peak close to the origin of the diagram, and by contours that diverge slightly away from the Hu axis, but eventually intersect the axis (Fig. 10C). This is characteristic of PSD behaviour [Roberts et al., 2000]. Samples SPAII-4b and SPAII-6 (not shown in Figure 10) are similar to the previous two, but there is an extra high coercivity component with very little spreading on the vertical axis, extending up to about 30 mT. This could be the hallmark of stable SD particles with little interaction. Finally, sample SPAII-5b is characterized by a very narrow peak close to the origin that also extends up to 30 mT (Fig. 10C), which indicates the presence of a mixture of stable SD and SP particles with a relaxation time comparable to the measuring time. It is fairly similar to the Yucca Mountain ash flow tuff that contains a substantial SP component shown in Roberts et al [2000]. The FORC diagrams from speleothem SPA are also characteristic of a SD-SP mixture for sample SPA-3 (Fig. 10C) and a mixture of SD with either a PSD or a SP component for sample SPA-9. The mixture of SD and SP grains could be also identified by checking whether the hysteresis loop is wasp-waisted (Fig. 10B). In the present case, the loop is not very open, but it seems to be slightly wasp-waisted.

These measurements indicate that the magnetic mineralogy in speleothem SPAII and in the reddish external rim of speleothem SPA is mostly dominated by fine grains ranging from SP to PSD. This is consistent with previous speleothem studies (see review by *Lascu and Feinberg*, 2011). It also seems that the grain size distribution varies significantly between the different laminations. However, results for the SPA are biased by the fact that only the outer altered layers were ferromagnetic enough to be measured.

7. Natural Remanent Magnetization (NRM)

In order to evaluate whether a paleomagnetic signal is preserved in fresh as well as weathered speleothems, we conducted paleomagnetic analysis. Samples from the weathered speleothem (SPA) are characterized by a very low NRM intensity (~10^{-4}A/m) and yield chaotic and unreliable magnetic vectors after AF cleaning (Fig. 11). In contrast, the fresh stalagmite (SPAII) carries a relatively high-intensity NRM (~10^{-2} to 10^{-3} A/m) and shows well-defined magnetic vectors decaying to the origin with maximum angular deviations (MAD) varying from 2.2º to 3.8º (Fig. 11). Magnetic directions are located in the same region of the stereographs (NNE-NE directed with inclination of ~25-30º). The NRM intensity is one order

of magnitude higher in the brown (SPAII-2) than in the white (SPAII-1 and SPAII-3) laminations suggesting that the lamination color is partially linked to the concentration of iron oxides (Fig. 11). Orthogonal projections show mostly univectorial vectors pointing to the origin for samples SPAII_1 and SPAII_2 whereas SPAII_3 shows a bimodal distribution of magnetic vectors but for which directions are almost similar (Fig. 11). Values of mean demagnetizing fields are around 15mT suggesting low coercivity ferromagnetic particles as principal magnetic carriers.

8. Visible Diffuse Reflectance Spectrophotometry (DRS)

Visible DRS analyses were conducted on SPAII samples (fresh stalagmite). Color is represented by CIE *L (lightness/darkness), CIE a* (green/red) and CIE b* (blue/yellow) curves (*CIE*, 1978) that are illustrated in Figure 12. The visible changes from white and light-brown (top) to dark-brown (base) color of the calcite laminae (see photographs in Fig. 12) correspond to a decrease in lightness (CIE L*) and a relative increase in redness (CIE a*) and yellowness (CIE b*). Because iron oxides adsorb strongly in the ultraviolet (UV) and blue spectral regions but are strongly reflecting in the red and infrared (IR) regions [*Scheinost and Schwertmann*, 1999; *Scheinost et al.*, 1998; *Torrent and Barrón*, 2002], they are probably the main carriers of the CIE a* and CIE b* signal. This is illustrated by the positive correlation between CIE a* and CIE b* and the content in iron oxides estimated by SIRM values of components 1 (Fig. 12). Conversely, values of CIE*L, which are generally controlled by the content in organic matter and calcite [*Adkins et al.*, 1997], show no correlation with CaO content (%wt) (Fig. 12). Instead, CIE*L varies concomitantly with concentration-dependent magnetic proxies (MS, SIRM) suggesting that iron oxides may also contribute to the darkness in this case. Indeed, opaque minerals such as magnetite/maghemite exhibit dark to brown color [*Pan et al.*, 2000], and may thus partially contribute to the darkness of the laminae.

9. Major and trace elements

Content in major (in %wt) and trace (in ppm) elements of the fresh stalagmite are illustrated in Figure 12. Except for Ca, Mg, Si, Al, Na, Sr, Ba, V, Th and As, contents in all other major and trace elements are below the detection limit of the spectrometer (~<0.1; Table 3). Concerning measurable major elements, we distinguished chemical elements that originate

from water-rock interaction, such as Ca, Mg, and Sr (alkaline-earth elements), from those that reside in the detrital fraction such as Fe, Si, Al, V, Ni, As, Th and Ba (detrital elements).

Regarding the calcium, contents in CaO vary slightly between 55.7 to 56.9%wt. A slight but significant increase in CaO content is noted in the brown lower part of the speleothem (from samples SPAII_11 up to SPAII_7 in Figure 12), whereas CaO contents are almost constant (or slightly decreasing) in the white upper part (samples SPAII_8, 9, 10). Loss on ignition (LOI) values, which generally depend on the content in water, organic matter and carbonates, are relatively high (42.3 to 42.9%wt). However, organic matter content is very low and under the detection level of the spectrometer (~<0.1%wt). This suggests that, in the present case, LOI values mostly informed about water and carbonates content in this case, as illustrated by the similar trends in the LOI, CaO (%wt) and $\delta^{18}O$ curves in Figure 12. Sr and Mg contents are averaged to ~19ppm and 0.25%wt, respectively, and co-vary with CaO contents (Fig. 12; Table 3).

Fe and Ti contents are below the detection limit of the spectrometer, except for darker samples (SPAII_4b and SPAII-11), (Table 3). However, there is a clear increase in detrital elements (Al, Si, V, As, Th and Ba) contents related to the increase in darkness (CIE*L) and concentration-dependent magnetic proxies (MS, SIRM). For example, Fe is only measurable in the most brownish layer where detrital elements are the most concentrated (Fig. 12). This suggests that iron oxides concentration, detrital input and color are controlled by the same (environmental) parameters.

10. Discussion

10.1. Magnetic mineralogy of fresh vs. weathered speleothems: factors controlling the reliability of paleomagnetic and environmental data

Three main conditions are required to ensure reliable environmental and paleomagnetic data in speleothems: i) the magnetic carriers must be of a primary origin (i.e. detrital or chemical in the case that magnetic minerals precipitate at the same time as calcite growth); ii) the magnetic carrier content should be sufficient to yield measurable remanence intensities and iii) these magnetic minerals must have been preserved since their deposition. The present study shows two nice examples of stable versus unreliable magnetizations recorded in a fresh and in a weathered speleothem (Fig. 11), respectively, providing the opportunity to illustrate

and discuss the factors that control the reliability of paleomagnetic and environmental data in speleothems.

Nature and origin of the magnetic carriers of the studied speleothems

The main magnetic carrier of stable DRM in speleothems is thought to be detrital (titano)-magnetite [*Lascu and Feinberg,* 2011; *Latham et al.,* 1979; *Lean et al.,* 1995; *Morinaga et al.,* 1986; *Openshaw et al.,* 1997; *Osete et al.,* 2012; *Perkins,* 1996; *Perkins and Maher,* 1993; *Pruner et al.,* 2010; *Zhu et al.,* 2012]. To a lesser extent maghemite has also been suggested [*Brook et al.,* 2006; *Herries et al.,* 2006; *Latham et al.,* 1989] but its identification has remained ambiguous. Indeed, since magnetite and maghemite have overlapping coercivity spectra, their discrimination using classic coercivity-dependent magnetic proxies (IRM, ARM) is difficult.

In the present study, the similarity in coercivity- and thermal-dependent magnetic properties observed when comparing speleothems, terra rossa soils and cave sediments, argues for a common origin of the magnetic carriers contained in these samples. The magnetic carriers are identified principally as maghemite and/or magnetite, and hematite and goethite. Median NRM, IRM and ARM demagnetization fields near 15-20 mT and S-ratio near 1 suggest the presence of maghemite/magnetite in the SPA and SPAII speleothems (Table 2; Figs. 5-8). The presence of maghemite is also deduced from thermomagnetic curves but the identification of primary magnetite is hampered by significant mineralogical transformations during the heating process. Hematite and goethite are identified by using unmixing IRM curves, whereas thermomagnetic and FORC experiments were unsuccessful because of the very low magnetic susceptibility and low saturation magnetization of hematite and goethite. Because of its much higher saturation magnetization, magnetite dominates in the majority of magnetic measurements, including hysteresis and FORC, even if hematite contributes up to 90% in the mixture [*Carvallo et al.,* 2006; *Frank and Nowaczyk,* 2008]. Grain sizes estimated by using FORC diagram and hysteresis parameters indicated a mixture of SP and SD/PSD. SD/PSD particles may correspond to the detrital Ti-bearing iron oxides observed under SEM and identified as maghemite/magnetite by magnetic properties. Similarly, SP particles may correspond to very fine grained detrital magnetite generally produced by pedogenic processes [*Evans and Heller,* 2003; *Thompson and Oldfield,* 1986], but its accurate identification is not resolvable by using SEM and temperature-dependence analysis.

The common and detrital origin of the iron oxides preserved in the studied set of samples is evidenced by: i) similar shapes of thermomagnetic curves from terra rossa soils, cave sediment and the fresh stalagmite from the Excentricas cave, as well as from the weathered stalactite from the Penico cave; ii) low dispersion of $B_{1/2}$ and DP values of the IRM component 1 (maghemite/magnetite) indicating a homogeneous population of grain size and coercivity spectra, probably resulting from an effective selection of detrital particles during transport or even at the source; iii) presence of zircon, and of Ti in iron oxides, deposited by drip-waters on the glass plates (Penico cave); iv) eroded shapes of the Ti-bearing iron oxide crystals in glass plates and speleothems observed under SEM microscope.

Features observed in the Portuguese speleothems under study would thus fulfill one of the prerequisites to secure reliable environmental records and paleomagnetic data in speleothems, namely a primary and detrital origin of the magnetic carriers. On the other hand, the weathered stalactite showed unreliable paleomagnetic results suggesting that other factors may play a role in the quality of the magnetic signal recorded in the speleothems under study.

Iron oxide alteration in speleothems: biotic or abiotic processes?

Several hypotheses can be proposed to explain the chaotic character of the magnetic directions isolated in the weathered stalactite: i) different remanence acquisition mechanisms varying between stalagmite and stalactite; ii) abiotic post-depositional chemical weathering mediated by change in water chemistry and cave environment, and/or iii) microbially-induced alteration (bioweathering). Although both stalactites and stalagmites are considered as speleothems, their formation and internal structures are different [see review in *Fairchild and Baker*, 2012]. In the case of stalactites, their growth is due to the water transport through a central canal inside the structure. Accordingly, stalactites usually start as being a soda straw type stalactite evolving into common tapered or carrot-shaped stalactites generally due to either a partial or complete blockage of the canal. Such growth and structure should strongly influence the orientation of the magnetic minerals and the resulting remanence. However, this hypothesis cannot be tested here because we did not have authorization to collect fresh stalactites for comparison. The second and third hypotheses are discussed as follows.

Factors controlling calcite dissolution in speleothems are well documented in the literature [e.g. *Fairchild et al.*, 2006], but little is known about abiotic alteration of iron oxides in speleothems. For example, magnetite has very long residence times (several millions of

years) when subjected to present-day weathering conditions (pH=5.6) but can be almost totally dissolved in some thousands of years at lower pH [*Symonds et al.*, 1992; *White et al.*, 1994]. On the other hand, whereas drip-waters often derive from epikarstic reservoirs of year-round constant pCO_2 [*Fairchild et al.*, 2000; *Fairchild et al.*, 2006], pCO_2 (and thus pH) of cave air can show significant seasonal variations. In order to evaluate this possibility, we modeled the influence of cave pH variations in cave on the dissolution of iron oxides such as maghemite. We use the PHREEQC program [*Parkhurst and Appelo*, 1999] developed by the U.S. Geological Survey for modeling water-rock interactions, coupled with the Wateq4f database [*Ball and Nordstrom*, 1991] with the following assumptions: (1) chemical equilibrium is reached between gas (O_2 and CO_2), liquid phase and solids, liquid and solid phases; (2) temperature in the cave is supposed constant and equal to 15°C; (3) CO_2 partial pressure varies between $10^{-3.4}$ bars corresponding to present day value and $10^{-1.5}$ bars similar to that of soils with biological activities [*Berner and Berner*, 1996]. Redox state (Eh) of the solution is controlled by the oxygen partial pressure. The chemical reactions involved in this system are:

$Fe_2O_3(s)$ [maghemite] + $3H^+ = 2Fe^{3+} + 3H_2O$

$CaCO_3(s)$ [calcite] + $H^+ = Ca^{2+} + HCO_3^-$

$CO_2(g) = CO_2(aq)$

$O_2(g) = O_2(aq)$

$CO_2(aq) + H_2O = H^+ + HCO_3^-$

$HCO_3^- = H^+ + CO_3^{2-}$

$Ca^{2+} + CO_3^{2-} = CaCO_3(s)$

where (s) stands for solid, (g) for gaseous and (aq) for aqueous.

The reaction pathway is as follows: protons given by CO_2 dissolution (weak acid) in water promote the dissolution of calcite and maghemite. Calculations show that the pH is buffered by calcite dissolution (lowest value is 6.98 for $pCO_2 = 10^{-1.5}$). The results displayed in Figure 13 show that the number of dissolved moles of maghemite needed to reach equilibrium increases with the pCO_2, as expected because of the more acidic conditions. Nevertheless, because of the near neutral pH conditions, this quantity remains very low compared to the 2.10^{-3} moles of maghemite in the SPA samples. Even for lower or greater temperatures (the

case corresponding to T=5°C), the quantity of dissolved maghemite remains very low (< 10^{-8} moles).

These results suggest that the chemical variations of the cave environment alone cannot explain the loss of iron oxides in the weathered speleothem and a microbial model is hypothesized.

Influence of microbial activity in the Penico cave is evidenced here by the widespread development of fungi (Mortierella) communities in present-day active calcite fabrics (on the watch plate) and by the close association between moon-milk, spiky calcite and needle-fiber calcite observed in the weathered stalactite under SEM microscope (Figs. 2-3). Interestingly, except for the external rim (SPA3 and SPA9), which showed IRM intensities comparable to those of the fresh stalagmite, samples affected by calcite dissolution and recrystallization (moon-milk) systematically exhibit lower (one to two order lower) IRM intensities than the fresh stalagmite (Figs. 7-8). The same is observed in NRM intensities of the two samples treated by AF cleaning (SPA6 and SPA10; Fig. 11). Thermomagnetic analyses and SEM observations of these samples also proved to be unsuccessful because of extremely low ferromagnetic content. We thus hypothesized that the weak remanent intensities of the weathered stalactite result from iron oxide dissolution directly or indirectly induced by fungal activity.

Interactions between fungi such as *Mortierella* and calcite fabrics (a field known as geomycology) are well documented in the literature [*Barton and Northup*, 2007; *Bindschedler et al.*, 2012; *Braissant et al.*, 2012; *Canaveras et al.*, 2006; *Cañaveras et al.*, 2001; *Gadd*, 1999; *Hoffland et al.*, 2004; *Kostka and Nealson*, 1995; *van Scholl et al.*, 2008], but little is known about the role played by microorganisms in the dissolution and neoformation of iron oxide in speleothem. More specifically, iron is a metal required by most microorganisms and is prominently used in the transfer of electrons during metabolism [*Howard*, 2004]. The processes involved in fungal activity and growth of fungal hyphal tips can produce organic proton- or ligand-based agents, such as metal oxalates and citrates, which lower the free cation activity and promote mineral dissolution [*Gadd*, 1999]. This would explain the halo of iron oxidation surrounding iron oxide host observed under optical microscope (Fig. 3B). Such observations suggest that fungal activity is a possible mechanism to explain the apparent reduced level of iron oxides observed in the weathered stalactites and the concomitant low values of remanent magnetization. Despite that our study concerns only

two samples and thus cannot be taken as a rule, such aspects should be taken into consideration for future paleomagnetic and environmental magnetic studies in speleothems.

10.2. Environmental magnetic records of the fresh stalagmite

Here we discuss how the behavior of the magnetic properties relates to other environmental proxies such as stable isotopes, color and mineralogy, and how this environmental information is recorded in the fresh speleothem under study.

As we discussed previously, the main magnetic carriers of the analyzed speleothems are primary and detrital in origin, which means that, in the absence of any post-depositional alteration (bioweathering in the present case), their concentration and grain size can be linked to environmental and climatic processes acting on the rock-atmosphere interface (hydrological regime, vegetal cover, temperature, etc.). Interestingly, in the case of the fresh stalagmite (not affected by bioweathering), variations of concentration-dependent magnetic proxies (MS, SIRM comp. 1) show a similar trend as the color and content in detrital elements, whereas stable (C-O) isotope compositions and content in alkaline-earth elements vary independently (Fig. 12). This suggests that the two set of proxies are controlled by independent environmental factors.

Stable C and O isotope compositions of the fresh and weathered speleothems show comparable values with other speleothems worldwide, and $\delta^{18}O$ compositions are coherent with the longitudinal location of the caves (Fig. 5). Like magnetic properties, stable isotopes compositions are thus considered as primary. Interpretation of $\delta^{18}O$ data is generally complex but reflects regional and local factors (air temperature, precipitation, altitude, continentality and humidity) that also control calcite precipitation, under chemical equilibrium, in the cave. The covariation of $\delta^{18}O$ and alkaline-earth elements (CaO, LOI, Sr, Mg) observed in the fresh stalagmite (Fig. 12) suggests this. To test this hypothesis, we used the Sr/Ca and Mg/Ca ratios (Fig. 12). Sr and Mg are mainly derived from bedrock dissolution and are further incorporated in the calcite lattice. They are thus excellent indicators of calcite-water interaction [*Fairchild et al.*, 2006; *Kaufman et al.*, 1998]. For example, positive covariations of Sr/Ca and Mg/Ca ratios, with slope of ~0.9, are commonly ascribed to prior calcite precipitation [*Fairchild et al.*, 2000; *Fairchild et al.*, 2006; *McGillen and Fairchild*, 2005; *McMillan et al.*, 2005], and/or incongruent calcite dissolution [*Sinclair*, 2011]. Here we calculate the ratio of ln(Sr/Ca) over ln(Mg/Ca) and obtained a slope of 0.75. This suggests

that alkaline-earth elements and oxygen isotope composition of the fresh stalagmite are mainly controlled by calcite-water interaction (Fig. 12).

Independently, iron oxides are assumed to be inherited from the Terra Rossa soil, and so, to inform about physico-chemical processes acting at the rock (or soils)-atmosphere interface. This is evidenced in Figure 12 by a positive correlation between coercivity-dependent magnetic proxies (MS, SIRM) and concentration in detrital elements. For example, comparison between MS (m^3/kg), SIRM intensities and content in Si (%wt) yielded correlation factors of R^2=0.71 and R^2=0.74, respectively (by using a linear trend; Table 4). Interestingly, there is also a positive correlation between concentration-dependent magnetic proxies (MS and SIRM comp. 1) and the color (a* and b*) (Table 4).

As a rule, annual laminae in speleothems are delineated by differences in the color of calcite, whereby a couplet of light and dark calcite indicates a year's growth (note however that this aspect has recently been challenged by *Shen et al.* [2013]). The main agent responsible for the coloration of calcite speleothem is generally attributed to organic compounds (fulvic acids and humic material) [*Gascoyne*, 1977; *Lauritzen et al.*, 1986; *van Beynen et al.*, 2001; *White*, 1997; *White*, 1981]. Speleothem color can thus represent a valuable environmental proxy. Accessorily, and depending on the regional conditions, other agents can contribute to the color, like the presence of different detrital elements contained in the calcite laminae including iron oxides, rare earth and metal transition elements, or calcite porosity [*Genty*, 1992; *Genty et al.*, 1997; *Jex et al.*, 2008; *van Beynen et al.*, 2001; *White*, 1997]. In the case of the fresh stalagmite under study, we have no accurate information about the contribution of organic compounds in the coloration of the calcite growths, because organic matter concentration is extremely low, i.e. below the detection level of the spectrometer. In counterpart, the covariation of CIE parameters and coercivity-dependent magnetic proxies suggests that, even if calcite speleothem coloration by iron oxides is rare, it may occur such as in the present case. This is particularly possible in the case of very low content in organic matter and in the case of "dirty" speleothems, i.e. those for which U-Th radiometric dating is ineffective due to high content in detrital elements, such as is the case here (*Ghaleb et al.*, 2014).

In summary, the present case study shows that environmental magnetism is a promising tool to identify the nature and composition of the detrital source contributing to the magnetic mineralogy of speleothems and, indirectly, the processes acting at the rock-atmosphere interface.

11. Conclusions

- The present work shows that detrital particles, including iron oxides, contribute to the magnetic properties and color of the speleothems under study. The similarity of coercivity- and temperature-dependent magnetic properties between the speleothems, the terra rossa soils and the cave sediments, as well as the presence of detrital Ti-bearing iron oxides and zircon contained in present-day drip-waters (glass plate) suggest a detrital origin and local source (i.e. terra rossa soils) for magnetic carriers. The color and magnetic properties of speleothems can thus be directly linked to the source composition and to the environmental context of the depositional settings.
- Stable isotopic composition of South Portuguese speleothems is likely primary, and can thus be used as a robust climatic and environmental proxy. Color, concentration-dependent magnetic proxies (MS, SIRM), and detrital element concentrations show a positive correlation, controlled by the source composition and processes acting at the rock-atmosphere interface. Oxygen isotope compositions and alkaline-earth elements co-vary independently, probably reflecting calcite-water interaction processes in these caves.
- Unlike the fresh stalagmite, the weathered stalactite provides unreliable NRM directions and yields very low remanent intensities. We suggest that these low intensities resulted either from different remanence acquisition mechanisms between stalagmite and stalactite and/or from iron dissolution by fungal activity. The presented numerical modeling suggests that chemical dissolution of maghemite is hard to achieve through abiotic processes in the case of the Penico Cave. However, the close association between moon-milk, widespread needle-fiber calcite and dissolution features of iron oxides indicate that fungal activity may contribute to iron oxide dissolution and loss of remanence.

AKNOWLEDGEMENTS

Funding was provided by PTDC/CTE-GIX/117298/2012 funded by FCT. We thank Celia Lee and Ana Sousa for administrative support, Susana Fernandes for her help in measurements. We want to acknowledge the two regional speleology associations that helped collecting the samples, namely CEEAA for the speleothem and GEONAUTA for the glass plates. We thank Fabio Florindo and Alexandra Abrajevitch for internal review of the

manuscript. We are grateful to Rob Van der Voo and Mathew Domeier for help with English grammar and orthography. We also thank Joshua Feinberg, Ioan Lascu, an anonymous reviewer and the associate editor Stuart Gilder for extremely useful comments that helped to improve the manuscript.

REFERENCES

Abrajevitch, A., and K. Kodama (2011), Diagenetic sensitivity of paleoenvironmental proxies: A rock magnetic study of Australian continental margin sediments, *Geochemistry Geophysics Geosystems*, *12*(5), 1-18.

Adkins, J. F., E. A. Boyle, L. Keigwin, and E. Cortijo (1997), Variability of the North Atlantic thermohaline circulation during the last interglacial period, *Nature*, *390*(6656), 154-156.

Bailey, M. E., and D. J. Dunlop (1983), Alternating-Field Characteristics of Pseudo-Single-Domain (2-14 Mu-M) and Multidomain Magnetite, *Earth Planet Sc Lett*, *63*(3), 335-352.

Ball, J. W., and D. K. Nordstrom (1991), User's manual for WATEQ4F, with revised thermodynamic data base and test cases for calculating speciation of major, trace, and redox elements in natural waters, *U.S. Geological Survey Open-File Report 91-183*, 189 p.

Barton, H. A., and D. E. Northup (2007), Geomicrobiology in cave environments: Past, current and future perspectives, *J Cave Karst Stud*, *69*(1), 163-178.

Bellanca, A., S. Hauser, R. Neri, and B. Palumbo (1996), Mineralogy and geochemistry of Terra Rossa soils, western Sicily: Insights into heavy metal fractionation and mobility, *Sci Total Environ*, *193*(1), 57-67.

Berner, E. K., and R. A. Berner (1996), Global Environment: Water, Air, and Geochemical Cycles, Prentice Hall, Upper Saddle River, NJ., pp. 396.

Bindschedler, S., L. Milliere, G. Cailleau, D. Job, and E. P. Verrecchia (2012), An Ultrastructural Approach to Analogies between Fungal Structures and Needle Fiber Calcite, *Geomicrobiol J*, *29*(4), 301-313.

Braissant, O., S. Bindschedler, A. U. Daniels, E. P. Verrecchia, and G. Cailleau (2012), Microbiological Activities in Moonmilk Monitored Using Isothermal Microcalorimetry (Cave of Vers Chez Le Brandt, Neuchatel, Switzerland), *J Cave Karst Stud*, *74*(1), 116-126.

Brook, G. A., B. B. Ellwood, L. B. Railsback, and J. B. Cowart (2006), A 164 ka record of environmental change in the American Southwest from a Carlsbad Cavern speleothem, *Palaeogeography Palaeoclimatology Palaeoecology*, *237*(2-4), 483-507.

Canaveras, J. C., S. Cuezva, S. Sanchez-Moral, J. Lario, L. Laiz, J. M. Gonzalez, and C. Saiz-Jimenez (2006), On the origin of fiber calcite crystals in moonmilk deposits, *Naturwissenschaften*, *93*(1), 27-32.

Cañaveras, J. C., S. Sanchez-Moral, V. Soler, and C. Saiz-Jimenez (2001), Microorganisms and microbially induced fabrics in cave walls, *Geomicrobiol J*, *18*(3), 223-240.

Cañaveras, J. C., M. Hoyos, S. Sánchez-Moral, E. Sanz-Rubio, J. Bedoya, V. Soler, I. Groth, P. Schumann, L. Laiz, I. Gonzalez, and C. Saiz-Jimenez (1999), Microbial communities associated with hydromagnesite and needle-fiber aragonite deposits in a karstic cave (Altamira, northern Spain), *Geomicrobiol J*, *16*(1), 9-25.

Carvallo, C., A. R. Muxworthy, and D. J. Dunlop (2006), First-order reversal curve (FORC) diagrams of magnetic mixtures: Micromagnetic models and measurements, *Physics of the Earth and Planetary Interiors*, *154*(3-4), 308-322.

CIE (Commission Internationale de l'Éclairage) (1978). Recommendations on Uniform Color Spaces, Color-Difference Equations, Psychometric Color Terms. , Supplement no. 2 to Publ. no. 15, Colorimetry; Bureau Central de la CIE: Paris, 1978, 1-21.

Cisowski, S. (1981), Interacting Vs Non-Interacting Single Domain Behavior in Natural and Synthetic Samples, *Physics of the Earth and Planetary Interiors*, *26*(1-2), 56-62.

Cornell, R. M., and U. Schwertmann (2003), The Iron Oxides: Structure, Properties, Reactions, Occurrences, and Uses, *Wiley-VCH, Weinheim, Germany*.

Daeron, M., W. Guo, J. Eiler, D. Genty, D. Blamart, R. Boch, R. Drysdale, R. Maire, K. Wainer, and G. Zanchetta (2011), (CO)-C-13-O-18 clumping in speleothems: Observations from natural caves and precipitation experiments, *Geochim Cosmochim Ac*, *75*(12), 3303-3317.

Degawa, Y., and W. Gams (2004), A new species of Mortierella, and an associated sporangiiferous mycoparasite in a new genus, Nothadelphia, *Stud Mycol*(50), 567-572.

Doubrovine, P. V., and J. A. Tarduno (2006), Alteration and self-reversal in oceanic basalts, *Journal of Geophysical Research-Solid Earth*, *111*(B12).

Dunlop, D., and Ö. Özdemir (1997), *Rock Magnetism: Fundamentals and Frontiers*, Cambridge University Press, Cambridge.

Dunlop, D. J. (2002), Theory and application of the Day plot (M-rs/M-s versus H-cr/H-c) 2. Application to data for rocks, sediments, and soils, *Journal of Geophysical Research-Solid Earth*, *107*(B3).

Egli, R. (2004), Characterization of individual rock magnetic components by analysis of remanence curves, 1. Unmixing natural sediments, *Stud Geophys Geod*, *48*(2), 391-446.

Egli, R., and W. Lowrie (2002), Anhysteretic remanent magnetization of fine magnetic particles, *Journal of Geophysical Research-Solid Earth*, *107* (B10).

Egli, R. (2013) VARIFORC: An optimized protocol for the calculation of non-regular first-order reversal curve (FORC) diagrams. Global and Planetary Change, doi: 10.1016/j.gloplacha.2013.08.003

Ellwood, B. B., and W. A. Gose (2006), Heinrich H1 and 8200 yr BP climate events recorded in Hall's Cave, Texas, *Geology*, *34*(9), 753-756.

Evans, M. E., and F. Heller (2003), Environmental Magnetism: Principles and Applications of Enviromagnetics, *Academic, San Diego, Calif.*

Fairchild, I. J., A. Borsato, A. F. Tooth, S. Frisia, C. J. Hawkesworth, Y. M. Huang, F. McDermott, and B. Spiro (2000), Controls on trace element (Sr-Mg) compositions of carbonate cave waters: implications for speleothem climatic records, *Chemical Geology*, *166*(3-4), 255-269.

Fairchild, I. J., C. L. Smith, A. Baker, L. Fuller, C. Spotl, D. Mattey, F. McDermott, and Eimp (2006), Modification and preservation of environmental signals in speleothems, *Earth-Science Reviews*, *75*(1-4), 105-153.Fairchild, I. J., and A. Baker (2012), Speleothem Science: From Process to Past Environments, *Wiley-Blackwell eds.*, pp. 450.

Fanjat, G., P. Camps, V. Shcherbakov, F. Barou, M. T. Sougrati, and M. Perrin (2012), Magnetic interactions at the origin of abnormal magnetic fabrics in lava flows: a case study from Kerguelen flood basalts, *Geophys J Int*, *189*(2), 815-832.

Font, E., N. Youbi, S. Fernandes, H. El Hachimi, Z. Kratinova, and Y. Hamim (2011), Revisiting the magnetostratigraphy of the Central Atlantic Magmatic Province (CAMP) in Morocco, *Earth Planet Sc Lett*, *309*(3-4), 302-317.

Frank, U., and N. R. Nowaczyk (2008), Mineral magnetic properties of artificial samples systematically mixed from haematite and magnetite, *Geophys J Int*, *175*(2), 449-461.

Frisia, S., A. Borsato, I. J. Fairchild, and F. McDermott (2000), Calcite fabrics, growth mechanisms, and environments of formation in speleothems from the Italian Alps and southwestern Ireland, *J Sediment Res*, *70*(5), 1183-1196.

Gadd, G. M. (1999), Fungal production of citric and oxalic acid: Importance in metal speciation, physiology and biogeochemical processes, *Adv Microb Physiol*, *41*, 47-92.

Ghaleb, B., C. Veiga-Pires, D. Moura, and C. Hillaire-Marcel (2014), Multi-proxy constraints on ages of low U-content , young and "dirty" speleothems: Example from southern Portugal cave deposits. Geophys. Res. Abstr. 16, 7141.

Gascoyne, M. (1977), Trace element geochemistry of speleothems, *Proceedings of the 7th Intern. Speleol. Congress, Sheffield, England*, 205-207.

Genty, D. (1992), Les spéléothèmes du tunnel de Godarville (Belgique), un exemple exceptionnel de concrétionnement moderne, intérêt pour l'étude de la cin~etique de précipitation de la calcite et de sa relation avec les variations d'environnements, *Spéléochronos*, *4*, 3-29.

Genty, D., A. Baker, and W. Barnes (1997), Comparaison entre les lamines luminescentes et les lamines visible annuelles de stalagmites, *Comptes-rendu de l'Académie des Sciences de Paris*, *325*, 193-200.

Halgedahl, S. L. (1998), Revisiting the Lowrie-Fuller test: alternating field demagnetization characteristics of single-domain through multidomain glass-ceramic magnetite, *Earth Planet Sc Lett*, *160*(3-4), 257-271.

Hanesch, M., H. Stanjek, and N. Petersen (2006), Thermomagnetic measurements of soil iron minerals: the role of organic carbon, *Geophys J Int*, *165*(1), 53-61.

Harrison, R. J., and J. M. Feinberg (2008), FORCinel: An improved algorithm for calculating first-order reversal curve distributions using locally weighted regression smoothing, *Geochemistry Geophysics Geosystems*, *9*.

Herries, A. I. R., J. W. Adams, K. L. Kuykendall, and J. Shaw (2006), Speleology and magnetobiostratigraphic chronology of the GD 2 locality of the Gondolin hominin-bearing paleocave deposits, North West Province, South Africa, *J Hum Evol*, *51*(6), 617-631.

Heslop, D., G. McIntosh, and M. J. Dekkers (2004), Using time- and temperature-dependent Preisach models to investigate the limitations of modelling isothermal remanent

magnetization acquisition curves with cumulative log Gaussian functions, *Geophys J Int*, *157*(1), 55-63.

Hill, C., and P. Forti (1997), Cave Minerals of the World, *National Speleological Society, (2nd Edition 1997) 463 pp. hardbound, ISBN 1-879961-07-5*.

Hoffland, E., et al. (2004), The role of fungi in weathering, *Front Ecol Environ*, *2*(5), 258-264.

Howard, D. H. (2004), Iron gathering by zoopathogenic fungi, *Fems Immunol Med Mic*, *40*(2), 95-100.

Jackson, M., P. Rochette, G. Fillion, S. Banerjee, and J. Marvin (1993), Rock magnetism of remagnetized Paleozoic carbonates - low-temperature behavior and susceptibility characteristics, *Journal of Geophysical Research-Solid Earth*, *98*(B4), 6217-6225.

Jex, C., E. Claridge, A. Baker, and C. Smith (2008), Hyperspectral imaging of speleothems, *Quatern Int*, *187*, 5-14.

Johnson, H. P., W. Lowrie, and D. V. Kent (1975), Stability of Anhysteretic Remanent Magnetization in Fine and Coarse Magnetite and Maghemite Particles, *Geophysical Journal of the Royal Astronomical Society*, *41*(1), 1-10.

Kaufman, A., G. J. Wasserburg, D. Porcelli, M. Bar-Matthews, A. Ayalon, and L. Halicz (1998), U-Th isotope systematics from the Soreq cave, Israel and climatic correlations, *Earth Planet Sc Lett*, *156*(3-4), 141-155.

Kostka, J. E., and K. H. Nealson (1995), Dissolution and Reduction of Magnetite by Bacteria, *Environ Sci Technol*, *29*(10), 2535-2540.

Krása, D., and J. Matzka (2007), Inversion of titanomaghemite in oceanic basalt during heating, *Physics of the Earth and Planetary Interiors*, *160*(2), 169-179.

Kruiver, P. P., M. J. Dekkers, and D. Heslop (2001), Quantification of magnetic coercivity components by the analysis of acquisition curves of isothermal remanent magnetisation, *Earth Planet Sc Lett*, *189*(3-4), 269-276.

Lachniet, M. S. (2009), Climatic and environmental controls on speleothem oxygen-isotope values, *Quaternary Sci Rev*, *28*(5-6), 412-432.

Lascu, I., and J. M. Feinberg (2011), Speleothem magnetism, *Quaternary Sci Rev*, *30*(23-24), 3306-3320.

Latham, A. G., H. P. Schwarcz, D. C. Ford, and G. W. Pearce (1979), Paleomagnetism of Stalagmite Deposits, *Nature*, *280*(5721), 383-385.

Latham, A. G., D. C. Ford, H. P. Schwarcz, and T. Birchall (1989), Secular Variation from Mexican Stalagmites - Their Potential and Problems, *Physics of the Earth and Planetary Interiors*, *56*(1-2), 34-48.

Lauritzen, S. E., D. C. Ford, and H. Schwarcz (1986), Humic substances in speleothem matrix, paleoclimate significance, *Proc. 9th Int. Cong. Speleology, Barcelona, Spain*, 77–79.

Lean, C. B., A. G. Latham, and J. Shaw (1995), Palaeosecular Variation from a Vancouver-Island Stalagmite and Comparison with Contemporary North-American Records, *J Geomagn Geoelectr*, *47*(1), 71-87.

Liu, Q. S., A. P. Roberts, J. C. Larrasoana, S. K. Banerjee, Y. Guyodo, L. Tauxe, and F. Oldfield (2012), Environmental Magnetism: Principles and Applications, *Reviews of Geophysics*, *50*.

Lu, S. G., L. Zhu, and J. Y. Yu (2012), Mineral magnetic properties of Chinese paddy soils and its pedogenic implications, *Catena*, *93*, 9-17.

McDermott, F., D. P. Mattey, and C. Hawkesworth (2001), Centennial-scale holocene climate variability revealed by a high-resolution speleothem delta O-18 record from SW Ireland, *Science*, *294*(5545), 1328-1331.

McDermott, F., T. C. Atkinson, I. J. Fairchild, L. M. Baldini, and D. P. Mattey (2011), A first evaluation of the spatial gradients in delta O-18 recorded by European Holocene speleothems, *Global Planet Change*, *79*(3-4), 275-287.

McDermott, F., S. Frisia, Y. Huang, A. Longinelli, B., Spiro, T. H. E., Heaton, C. J. Hawkesworth, A. Borsato, E. Keppens, I. J. Fairchild, K. van der Borg, S. Verheyden, and E. Selmo (1999), Holocene climate variability in Europe: Evidence from delta O-18, textural and extension-rate variations in three speleothems, *Quaternary Sci Rev*, *18*(8-9), 1021-1038.

McGillen, M. R., and I. J. Fairchild (2005), An experimental study of incongruent dissolution of CaCO3 under analogue glacial conditions, *J Glaciol*, *51*(174), 383-390.

McMillan, E. A., I. J. Fairchild, S. Frisia, A. Borsato, and F. McDermott (2005), Annual trace element cycles in calcite-aragonite speleothems: evidence of drought in the western Mediterranean 1200-1100 yr BP, *J Quaternary Sci*, *20*(5), 423-433.

Meert, J. G., F. D. Pruett, and E. Merino (2009), An "Inverse Conglomerate" Paleomagnetic Test and Timing of In Situ Terra Rossa Formation at Bloomington, Indiana, *J Geol*, *117*(2), 126-138.

Morinaga, H., H. Inokuchi, and K. Yaskawa (1986), Magnetization of a Stalagmite in Akiyoshi Plateau as a Record of the Geomagnetic Secular Variation in West Japan, *J Geomagn Geoelectr*, *38*(1), 27-44.

Morinaga, H., I. Horie, and K. Yaskawa (1992), A Geomagnetic Reversal Recorded in a Stalagmite Collected in Western Japan, *J Geomagn Geoelectr*, *44*(8), 661-675.

Openshaw, S., A. Latham, and J. Shaw (1997), Speleothem palaeosecular variation records from China: Their contribution to the coverage of Holocene palaeosecular variation data in east Asia, *J Geomagn Geoelectr*, *49*(4), 485-505.

Osete, M. L., J. Martin-Chivelet, C. Rossi, R. L. Edwards, R. Egli, M. B. Munoz-Garcia, X. F. Wang, F. J. Pavon-Carrasco, and F. Heller (2012), The Blake geomagnetic excursion recorded in a radiometrically dated speleothem, *Earth Planet Sc Lett*, *353*, 173-181.

Ozdemir, O. (1987), Inversion of Titanomaghemites, *Physics of the Earth and Planetary Interiors*, *46*(1-3), 184-196.

Pan, Y. X., R. X. Zhu, and S. K. Banerjee (2000), Rock magnetic properties related to thermal treatment of siderite: Behavior and interpretation (vol 105, pg 783, 200), *Journal of Geophysical Research-Solid Earth*, *105*(B4), 8389-8389.

Parkhurst, D. L., and C. A. J. Appelo (1999), User's guide to PHREEQC version 2 - A computer program for speciation, batch-reaction, one -dimensional transport, and inverse calculations. , *Water-Ressources Investigations Rep. , U.S. Geological Survey, Denver, Colorado.* , 99-4259, .

Perkins, A. M. (1996), Observations under electron microscopy of magnetic minerals extracted from speleothems, *Earth Planet Sc Lett*, *139*(1-2), 281-289.

Perkins, A. M., and B. A. Maher (1993), Rock Magnetic and Paleomagnetic Studies of British Speleothems, *J Geomagn Geoelectr*, *45*(2), 143-153.

Pruner, P., V. Housa, F. Oloriz, M. Kostak, M. Krs, O. Man, P. Schnabl, D. Venhodova, J. M. Tavera, and M. Mazuch (2010), High-resolution magnetostratigraphy and biostratigraphic zonation of the Jurassic/Cretaceous boundary strata in the Puerto Escano section (southern Spain), *Cretaceous Res*, *31*(2), 192-206.

Riechelmann, D. F. C., M. Deininger, D. Scholz, S. Riechelmann, A. Schroder-Ritzrau, C. Spotl, D. K. Richter, A. Mangini, and A. Immenhauser (2013), Disequilibrium carbon and oxygen isotope fractionation in recent cave calcite: Comparison of cave precipitates and model data, *Geochim Cosmochim Ac*, *103*, 232-244.

Roberts, A. P., C. R. Pike, and K. L. Verosub (2000), First-order reversal curve diagrams: A new tool for characterizing the magnetic properties of natural samples, *Journal of Geophysical Research-Solid Earth*, *105*(B12), 28461-28475.

Robertson, D. J., and D. E. France (1994), Discrimination of remanence-carrying minerals in mixtures, using Isothermal Remanent Magnetization acquisition curves, *Physics of the Earth and Planetary Interiors*, *82*(3-4), 223-234.

Scheinost, A. C., and U. Schwertmann (1999), Color identification of iron oxides and hydroxysulfates: Use and limitations, *Soil Sci Soc Am J*, *63*(5), 1463-1471.

Scheinost, A. C., A. Chavernas, V. Barron, and J. Torrent (1998), Use and limitations of second-derivative diffuse reflectance spectroscopy in the visible to near-infrared range to identify and quantify Fe oxide minerals in soils, *Clay Clay Miner*, *46*(5), 528-536.

Shen, C. C., K. Lin, W. H. Duan, X. Y. Jiang, J. W. Partin, R. L. Edwards, H. Cheng, and M. Tan (2013), Testing the annual nature of speleothem banding, *Sci Rep-Uk*, *3*.

Sinclair, D. J. (2011), Two mathematical models of Mg and Sr partitioning into solution during incongruent calcite dissolution Implications for dripwater and speleothem studies, *Chemical Geology*, *283*(3-4), 119-133.

Stock, G. M., D. E. Granger, I. D. Sasowsky, R. S. Anderson, and R. C. Finkel (2005), Comparison of U-Th, paleomagnetism, and cosmogenic burial methods for dating caves: Implications for landscape evolution studies, *Earth Planet Sc Lett*, *236*(1-2), 388-403.

Strauss, B. E., J. H. Strehlau, I. Lascu, J. A. Dorale, R. L. Penn, and J. M Feinberg (2013), The origin of magnetic remanence in stalagmites: Observations from electron microscopy and rock magnetism, *Geochemistry, Geophysics, Geosystems*, *14*, 5006-5025.Symonds, R. B., M. H. Reed, and W. I. Rose (1992), Origin, Speciation, and Fluxes of Trace-Element Gases at Augustine Volcano, Alaska - Insights into Magma Degassing and Fumarolic Processes, *Geochim Cosmochim Ac*, *56*(2), 633-657.

Thompson, R., and F. Oldfield (1986), Environmental Magnetism, *Allen and Unwin, London 1986. pp. 227*.

Torrent, J., and V. Barrón (2002), Diffuse Reflectance Spectroscopy of iron oxides, *Encyclopedia of Surface and Colloid Science*.

van Beynen, P., R. Bourbonniere, D. Ford, and H. Schwarcz (2001), Causes of colour and fluorescence in speleothems, *Chemical Geology*, *175*(3-4), 319-341.

van Scholl, L., T. W. Kuyper, M. M. Smits, R. Landeweert, E. Hoffland, and N. van Breemen (2008), Rock-eating mycorrhizas: their role in plant nutrition and biogeochemical cycles, *Plant Soil*, *303*(1-2), 35-47.

Vaughan, M. J., R. M. Maier, and B. M. Pryor (2011), Fungal communities on speleothem surfaces in Kartchner Caverns, Arizona, USA, *Int J Speleol*, *40*(1), 65-77.

Wang, L., W. Chen, Y. Feng, Y. Ren, Z. Gu, H. Chen, H. Wang, M. J. Thomas, B. Zhang, I. M. Berquin, Y. Li, J. Wu, H. Zhang, Y. Song, X. Liu, J. S. Norris, S. Wang, P. Du, J. Shen, N. Wang, Y. Yang, W. Wang, L. Feng, C. Ratledge, H. Zhang, and Y. Q. Chen (2011), Genome Characterization of the Oleaginous Fungus Mortierella alpina, *Plos One*, *6*(12).

White, W. B. (1997), Color of speleothems, *In : Hill C.A. and Forti P. (Eds.): Cave minerals of the world. National Speleological Society*, 239-244.

White, A. F., M. L. Peterson, and M. F. Hochella (1994), Electrochemistry and Dissolution Kinetics of Magnetite and Ilmenite, *Geochim Cosmochim Ac*, *58*(8), 1859-1875.

White, W. B. (1981), Reflectance Spectra and Color in Speleothems, *The National Speleological Society*, *43*(1), 20-26.

Xu, S., and D. J. Dunlop (1995), Toward a Better Understanding of the Lowrie-Fuller Test, *Journal of Geophysical Research-Solid Earth*, *100*(B11), 22533-22542.

Zhu, Z. M., S. H. Zhang, C. Y. Tang, H. Y. Li, S. C. Xie, J. L. Ji, and G. Q. Xiao (2012), Magnetic fabric of stalagmites and its formation mechanism, *Geochemistry Geophysics Geosystems*, *13*.

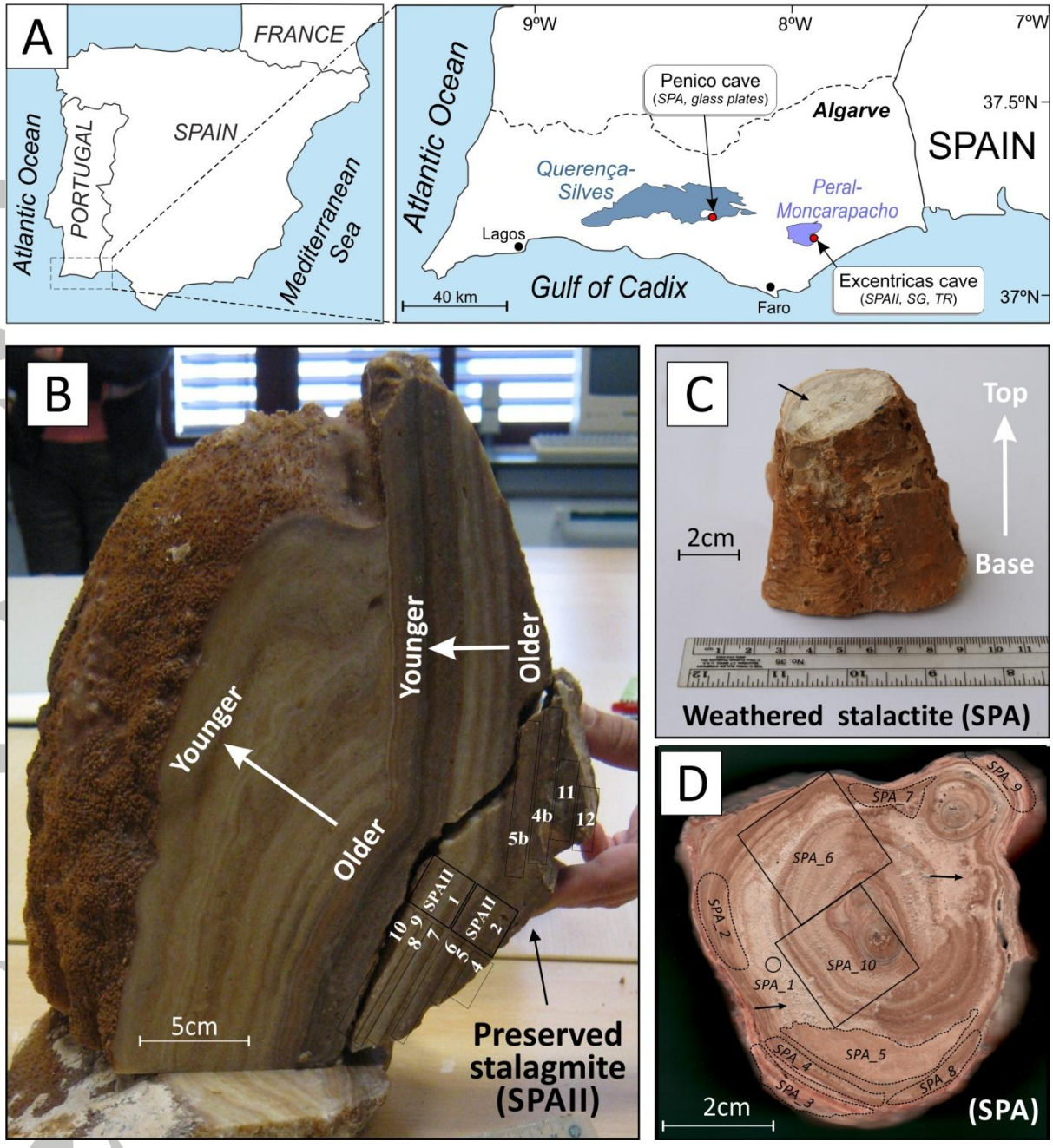

Figure 1. A) Geographic maps showing the location of the Algarve Basin (southern Portugal), the Querença-Silves and Peral-Moncarapacho aquifers and the corresponding caves (Penico and Excentricas) under study. SG and TR correspond to the cave sediments and terra rossa soils, respectively. B) Photographs of the fresh stalagmite (SPAII) showing the location of cubic samples (SPAII_1 and SPAII_2) extracted for paleomagnetic analysis and sub-samples (fragments of thin laminae; SPAII_4 to SPAII_12) collected for measurement of bulk magnetic properties. White arrows indicates the axial growth direction of calcite precipitation. C) Photographs of the weathered stalactite (SPA). The dark arrow indicates the direction from the ceiling (base) to the termination of the stalactite (top). D) Transversal section of SPA showing the location of cubic samples and sub-samples. The black arrows point to zones of calcite alteration (moon-milk).

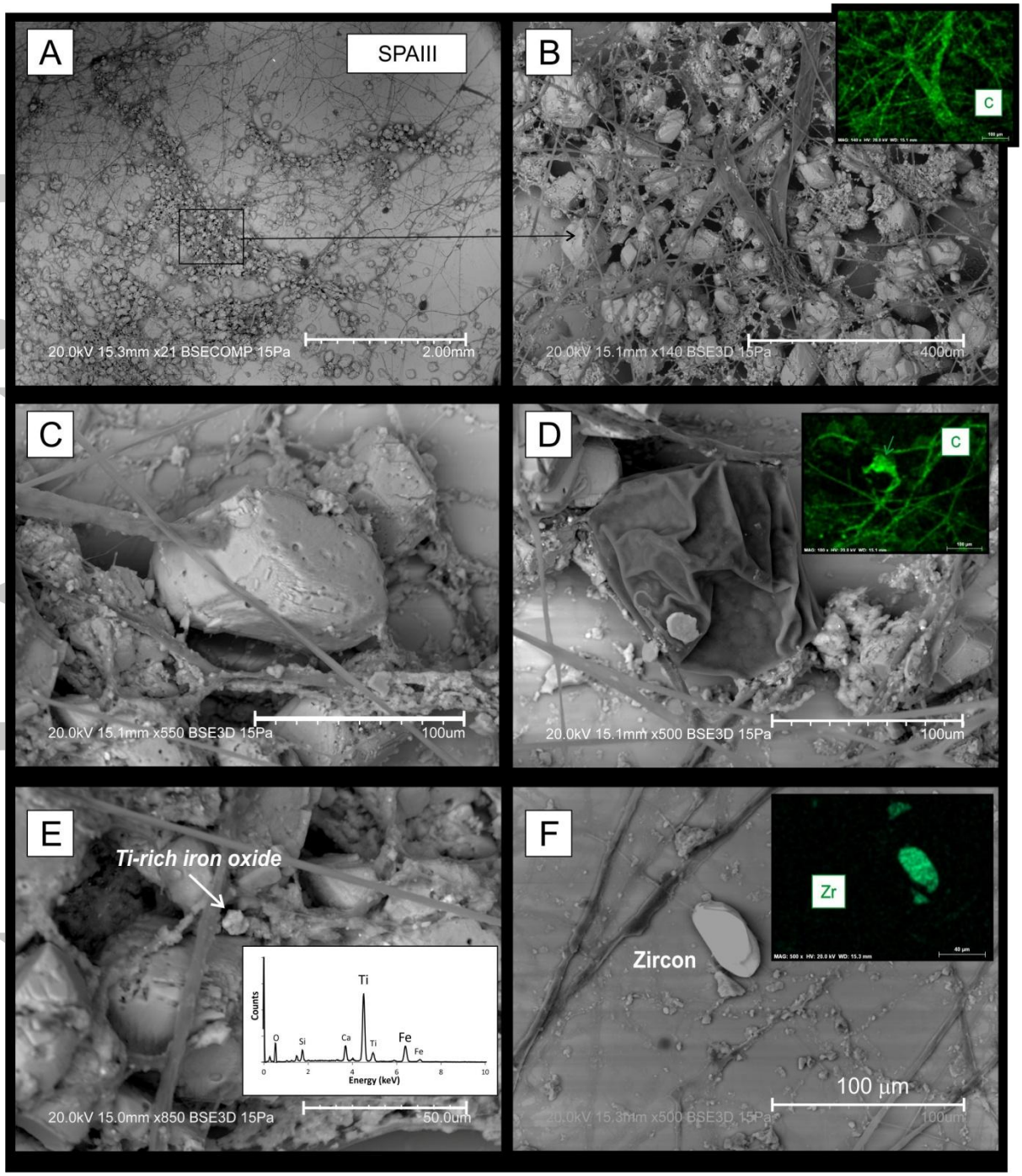

Figure 2. Scanning Electron Microscopy photographs of the watch glasses from the Penico cave (same cave as SPA stalactite). A) After three months in the cave, a widespread network of calcite and organic filaments similar to hyphae developed; B) Mapping electron microscopy reveals carbon as principal constituent of the filament; C) A calcite crystal has a rounded shape and serves as an anchor for the development of the fungal hyphae; D) Sporangiospore (flattened due to vacuum); E) Rare detrital Ti-Fe iron oxides are observed as well as F) detrital zircon.

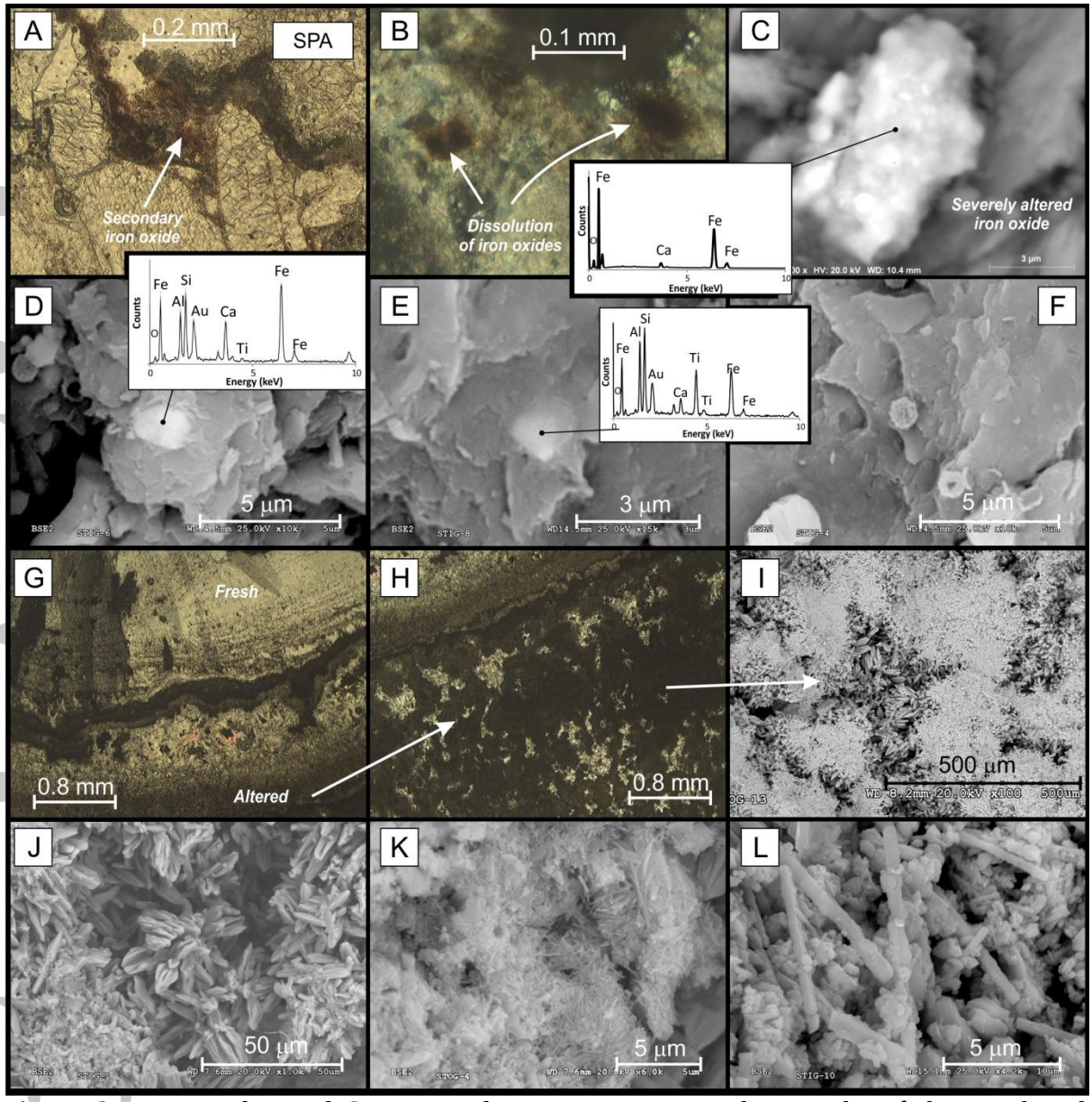

Figure 3. Petrographic and Scanning Electron Microscopy photographs of the weathered stalactite (SPA). A) Secondary iron filling intergranular spaces; B) Oxidized iron oxides; C) Severely altered iron oxide; D-E) Fe-Ti iron oxides included in detrital material (the Au peak on EDS spectra is due to gold coating during sample preparation); F) Spheroidal concretion (biogenic or cosmogenic?); G-H) Petrographic image showing the fresh and well laminated calcite laminae, as well as altered zones; I) Scanning electron microscopic image (back scattered and secondary) of altered zones showing J) spiky calcite locally recovered by K) biogenic calcite needle of less than 5 µm in length; L) Regions with microcrystalline calcite also affected by biomineralization and containing larger (~10 µm in length) calcite needles.

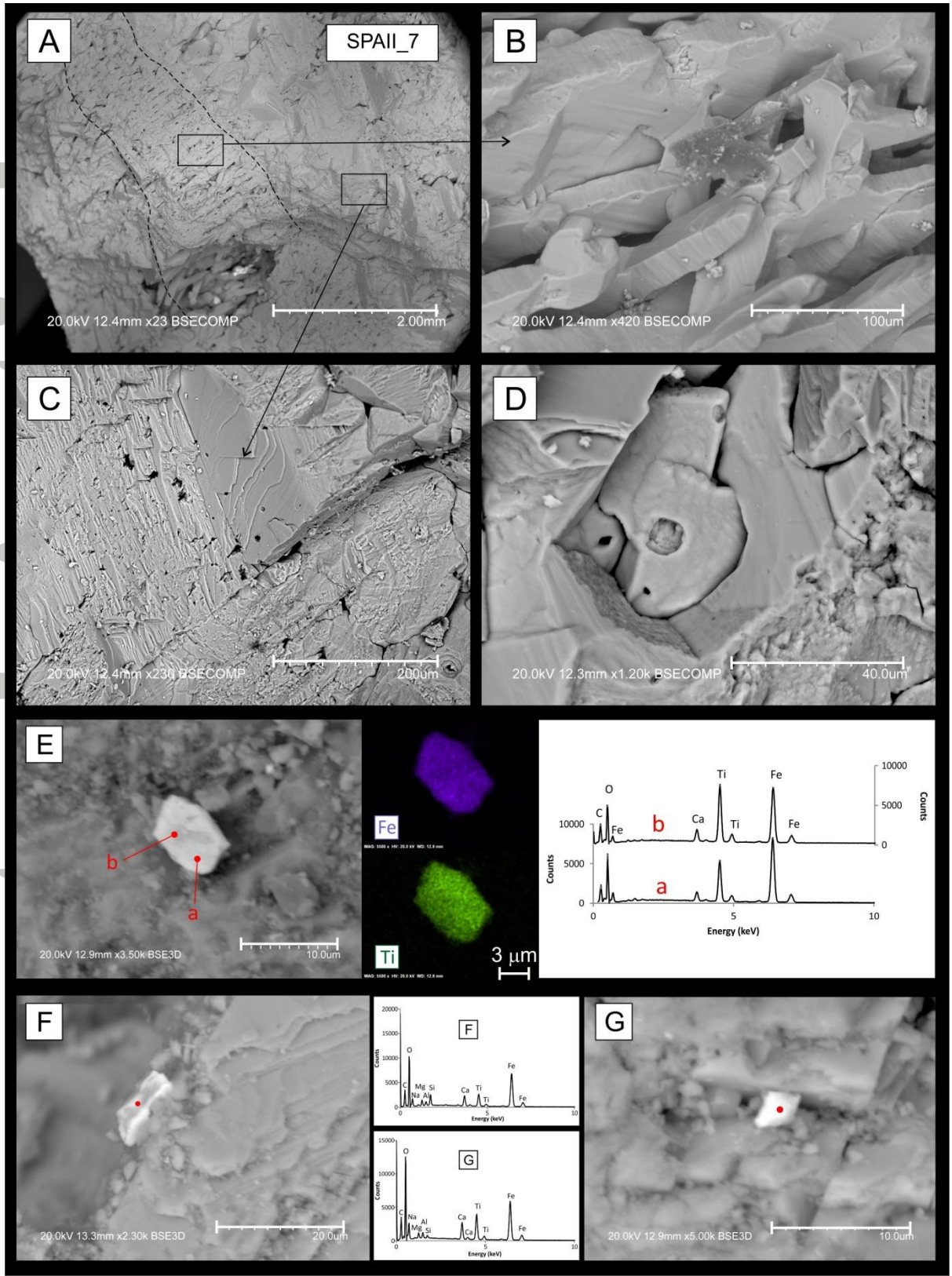

Figure 4. Scanning Electron Microscopy photographs of the fresh stalagmite from the Excentricas cave. A-C) The stalagmite presents a distinct calcite texture, which alternates with massive microcrystalline calcite to columnar calcite; D) some voids are observed on the surface of the calcite crystal and are interpreted as the result of fungal activity (fixation of hyphae); E-G) Composition mapping and EDS spectra of detrital Fe-Ti iron oxide with moderate to rich content in titanium.

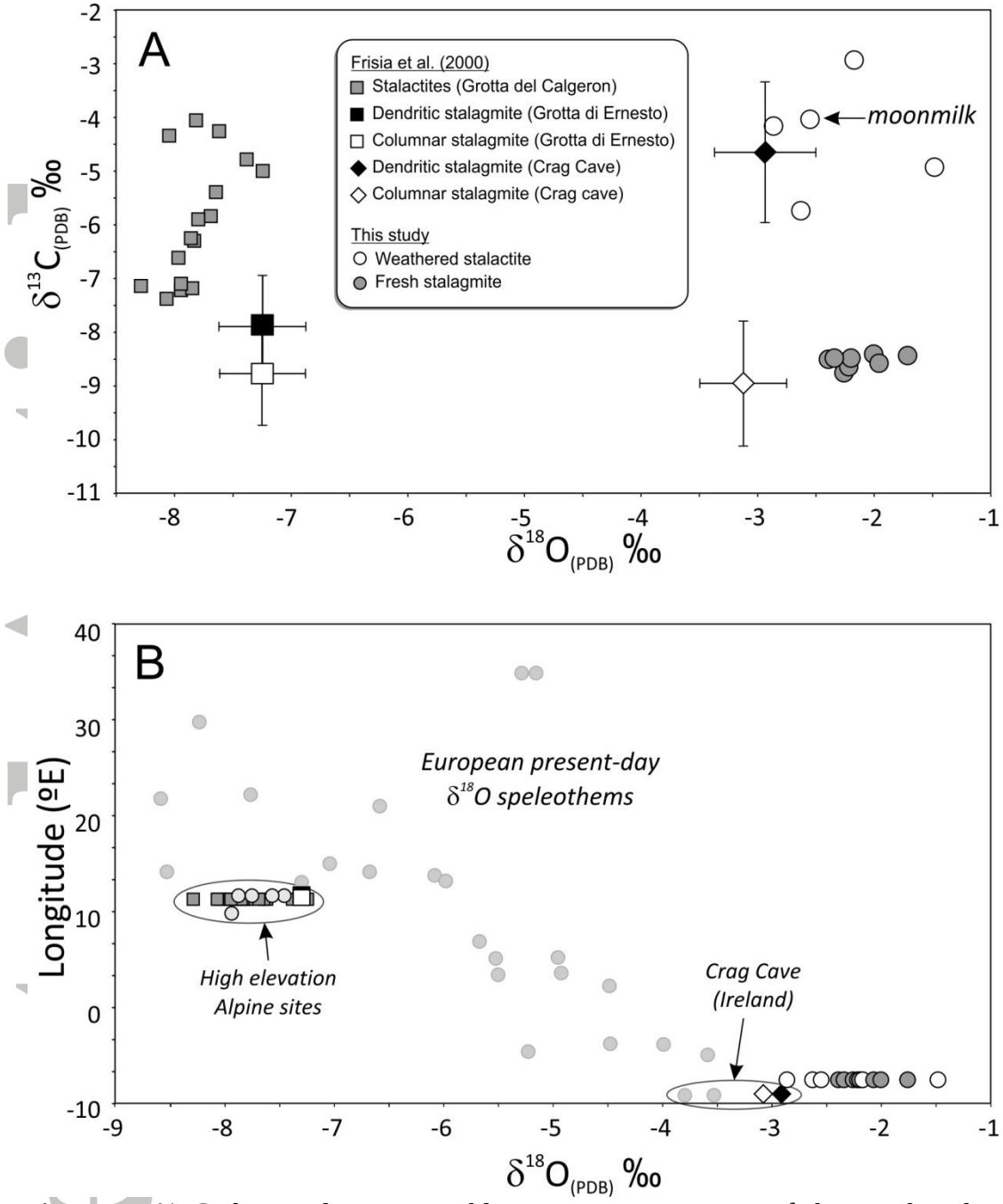

Figure 5. A) Carbon and oxygen stable isotopic composition of the weathered and fresh speleothems compared to speleothems from the Crag Cave (Ireland) and Grotta del Calgeron (Alpes) [modified from *Frisia et al.*, 2000]. Moon-milk (SPA1) from the weathered stalactite has similar values to other crystalline calcite samples. B) Present-day $\delta^{18}O_{speleothem}$ values against the longitude of European cave [*McDermott et al.*, 2011] and Portuguese speleothems (this study). Data from *Frisia et al.* [2000] are also shown.

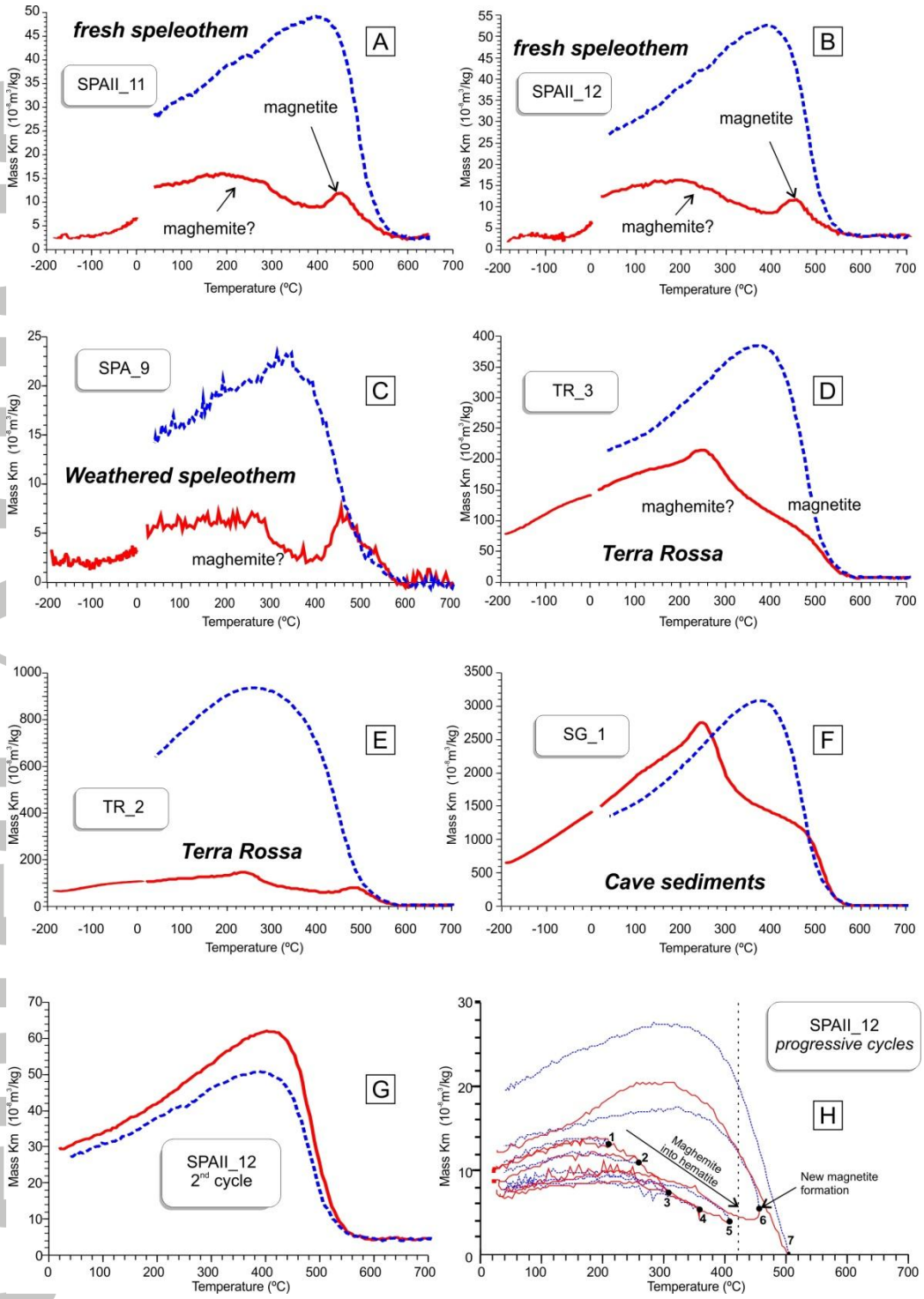

Figure 6. Low and high temperature thermomagnetic curves of A-B) the fresh stalagmite (samples SPAII_11 and SPAII_12), C) the weathered stalactite (sample SPA9), D-E) the terra rossa soils capping the cave (TR_2, TR_3) and F) cave sediments (SG_1). All heating cycles show a systematic increase in MS values from -196ºC up to 250ºC, interpreted as a gradual passing of the SD/SP threshold, and an abrupt decrease up to ~400ºC, in turn interpreted as the inversion of maghemite into hematite; G) second subsequent heating/cooling cycles of SPAII_12 show magnetite as final transformation product; H) Stepwise progressive heating/cooling cycles of SPAII_12 showing maghemite inversion into hematite until 400ºC and magnetite authigenesis above 400ºC. Steps 1, 2, 3, 4, 5, 6 and 7 correspond to heating/cooling cycles at 200, 250, 300, 350, 400, 450 and 500ºC, respectively.

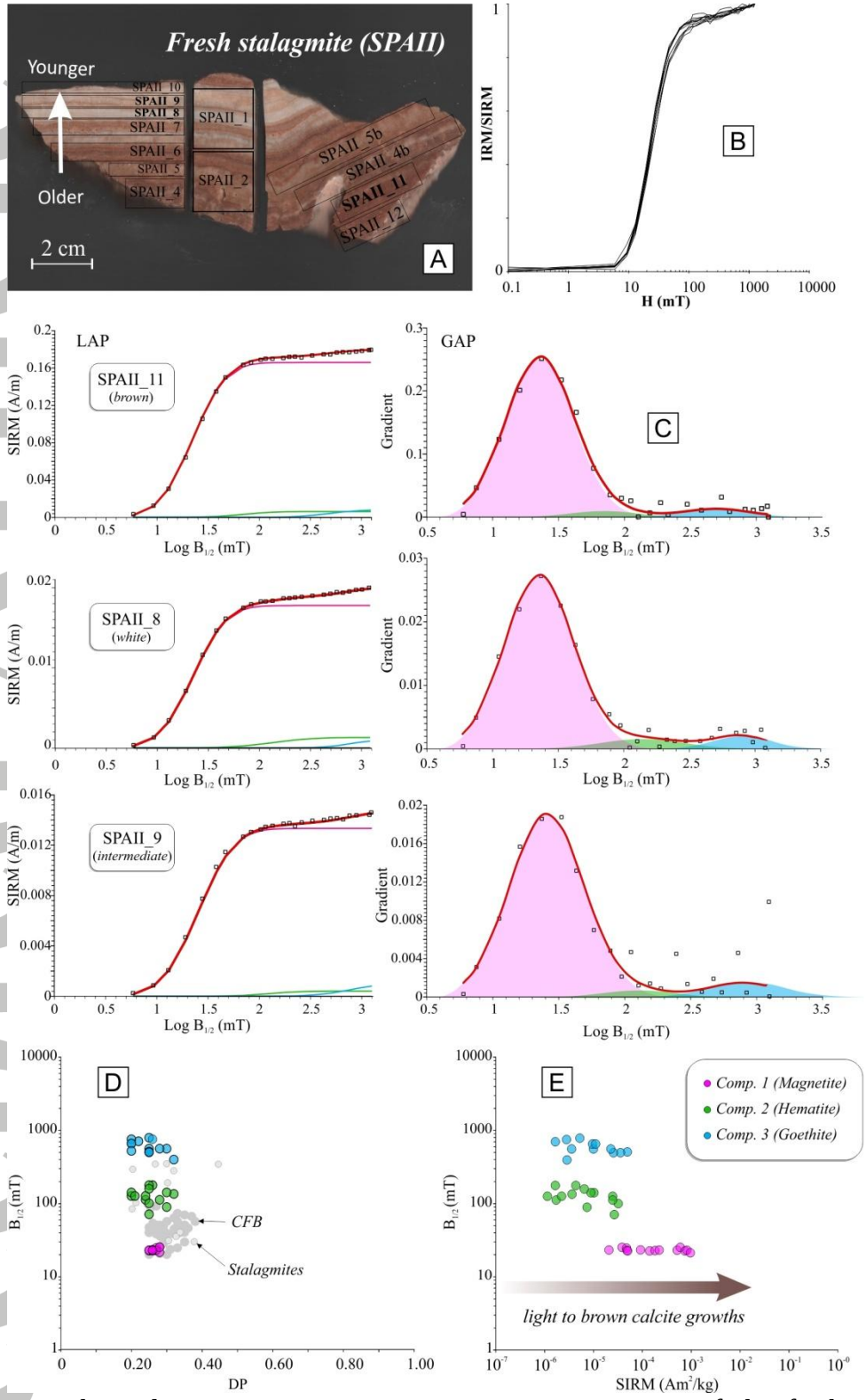

Figure 7. Isothermal remanent magnetization acquisition curves of the fresh stalagmite (SPAII) after treatment by the Cumulative Log-Gaussian function. A) Localization of samples; B) raw IRM/SIRM curves showing similar coercivity spectra; C) examples of linear (LAP) and gradient (GAP) acquisition plots; D) $B_{1/2}$ versus Dispersion Parameter (DP); E) $B_{1/2}$ versus Mass normalized SIRM. Shadowed grey and white circles in the background of graph (d) correspond to titanomagnetites from continental flood basalts (*Font et al.*, 2011; Font E., unpublished data) and stalagmites (*Lascu and Feinberg*, 2011).

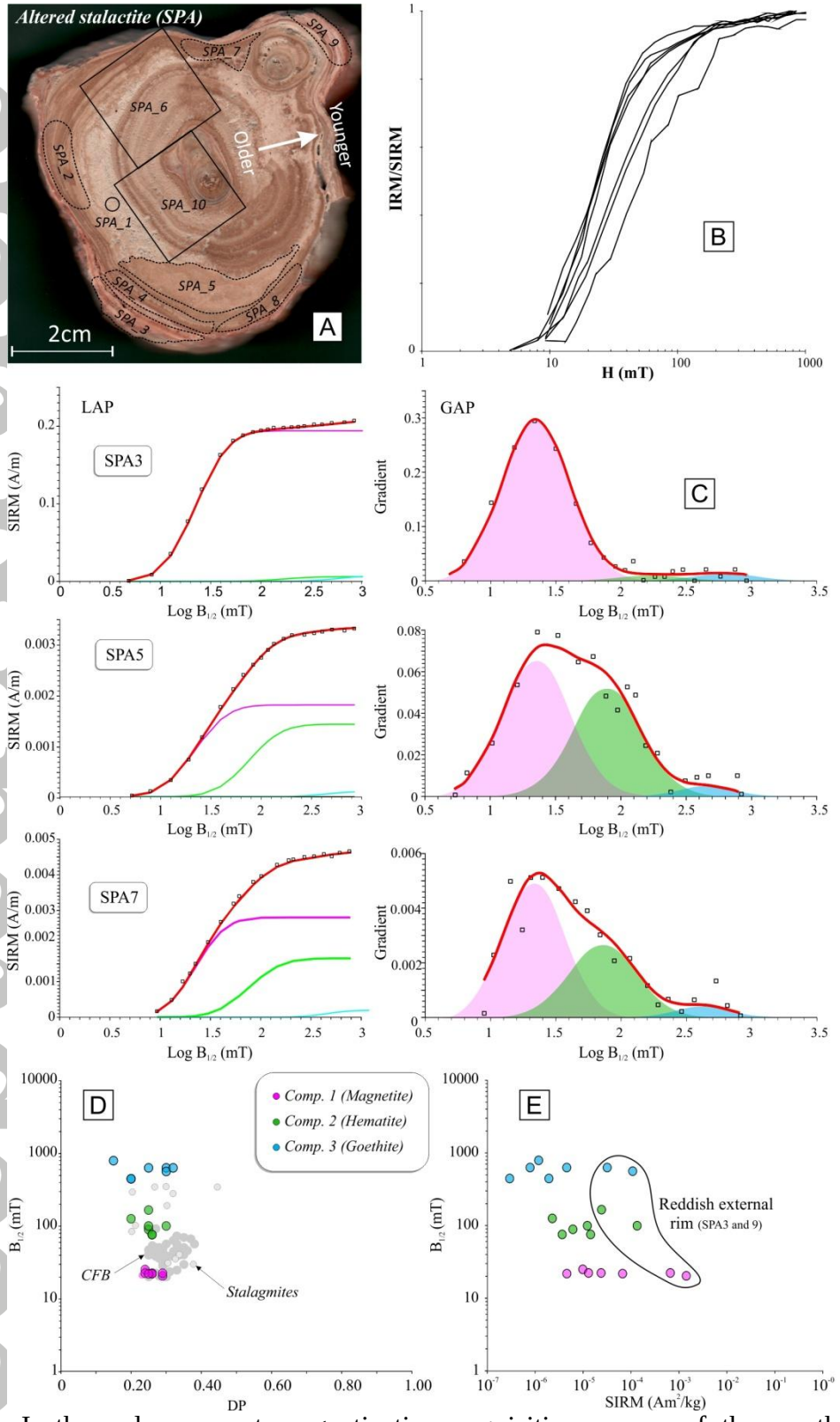

Figure 8. Isothermal remanent magnetization acquisition curves of the weathered SPA stalactite after treatment by the Cumulative Log-Gaussian function. A) Localization of samples; B) raw IRM/SIRM curves showing large variation in coercivity spectra; C) examples of linear (LAP) and gradient (GAP) acquisition plots; D) $B_{1/2}$ versus Dispersion Parameter (DP); E) $B_{1/2}$ versus SIRM/Mass. Shadowed grey and white circle in the background of graph (d) correspond to titanomagnetites from continental flood basalts (*Font et al.*, 2011; Font E., unpublished data) and stalagmites (*Lascu and Feinberg*, 2011).

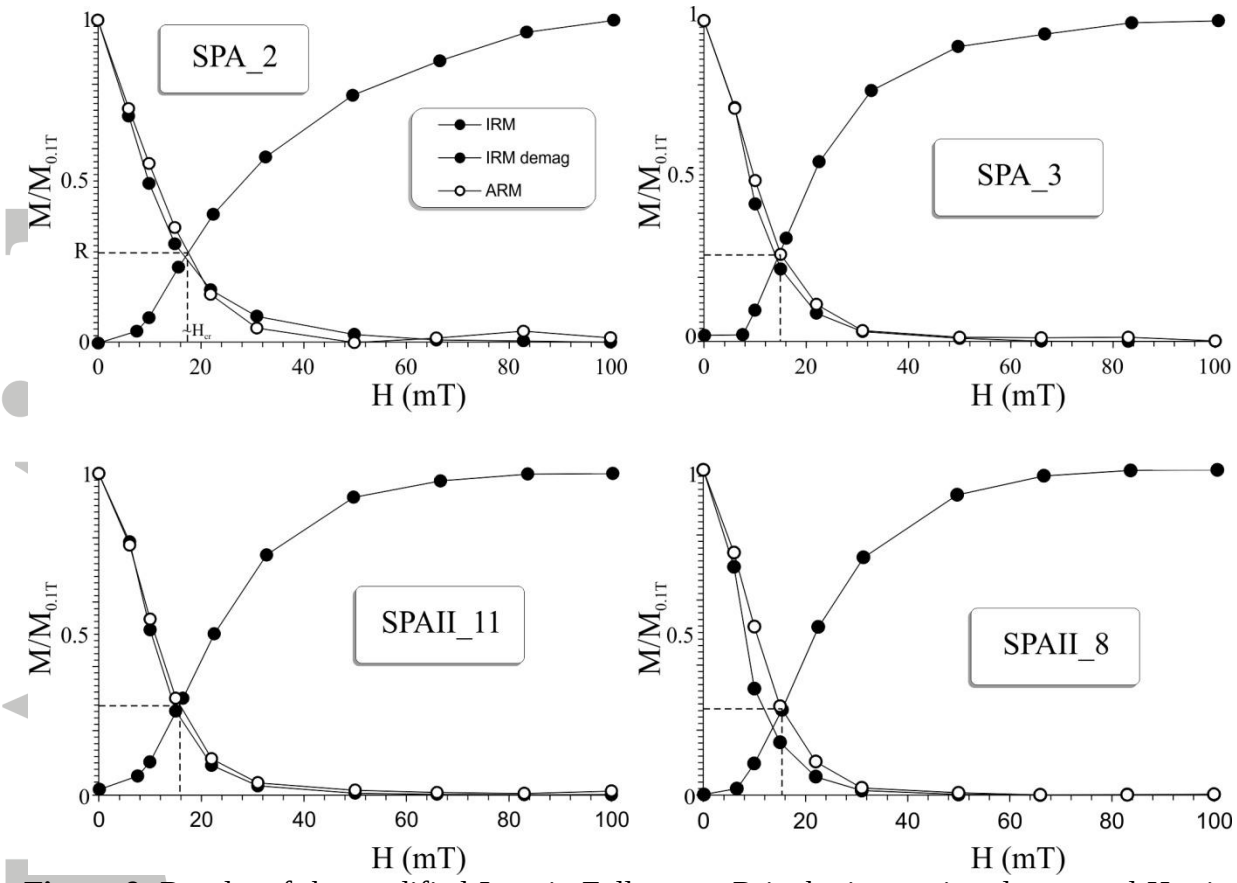

Figure 9. Results of the modified Lowrie-Fuller test. R is the interaction degree and Hrc is the remanent coercive force. Most samples gave a L-type result (ARM being harder to demagnetize than the IRM) in the Lowrie-Fuller test suggesting presence of monodomain (SD) magnetic particles. Coercivity (Hc) values estimated by using the Cisowski test are inferior to 20 mT indicating presence of low coercivity magnetic particles. R values are inferior to 0.5 indicating strong interaction of SD particles.

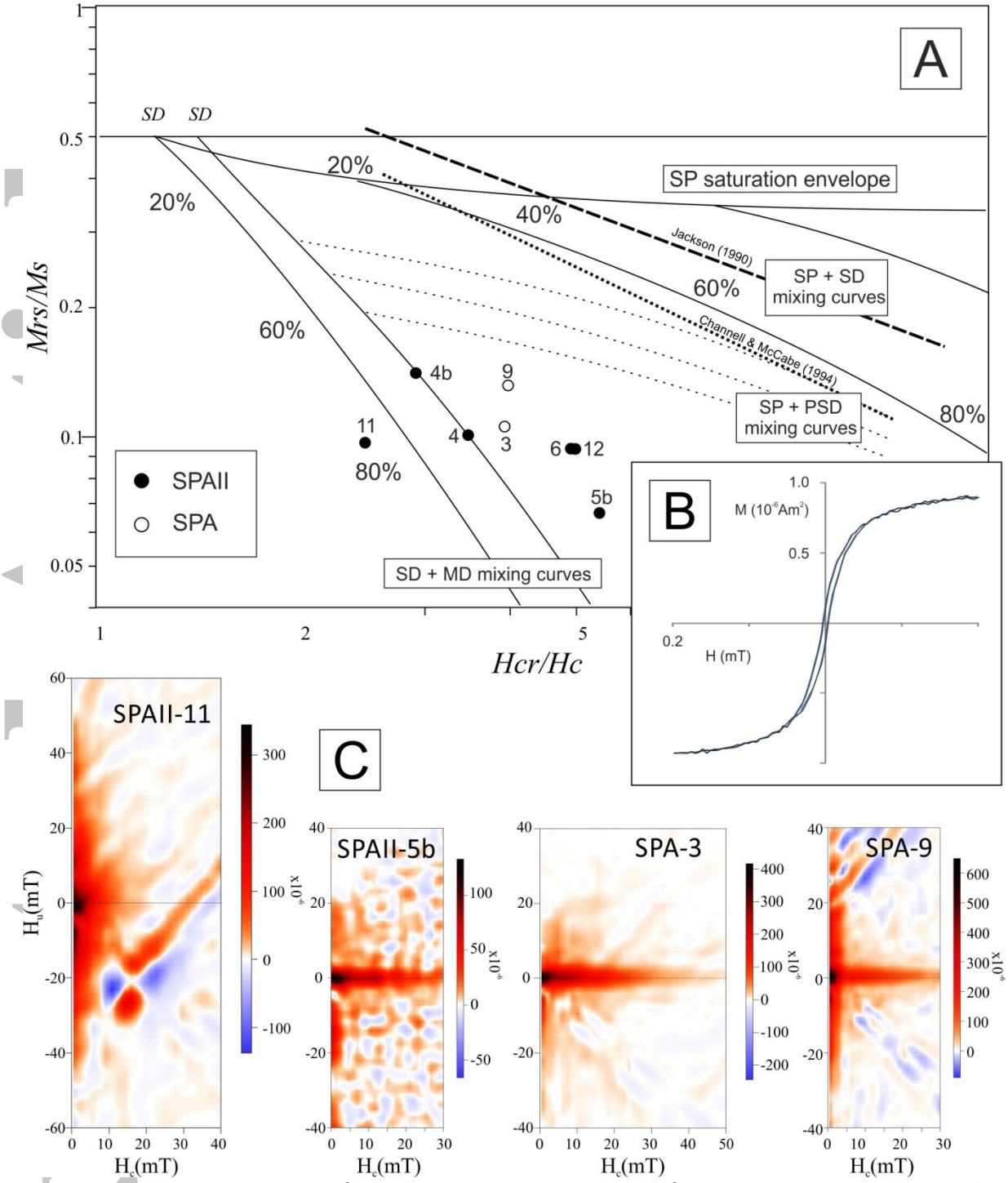

Figure 10. A) Hysteresis data from the weathered (SPA) and fresh (SPAII) speleothem under study plotted on the theoretical unmixing diagram of *Dunlop* [2002] and showing a typical SD+MD trend. Open/close symbols correspond to SPA/SPAII samples, respectively. B) Example of a wasp-waisted hysteresis loop (sample SPA-9). C) FORC diagrams of representative samples plotted with a variable smoothing factor (Egli et al., 2013). The H_c and H_u scales are the same for all the FORC diagrams.

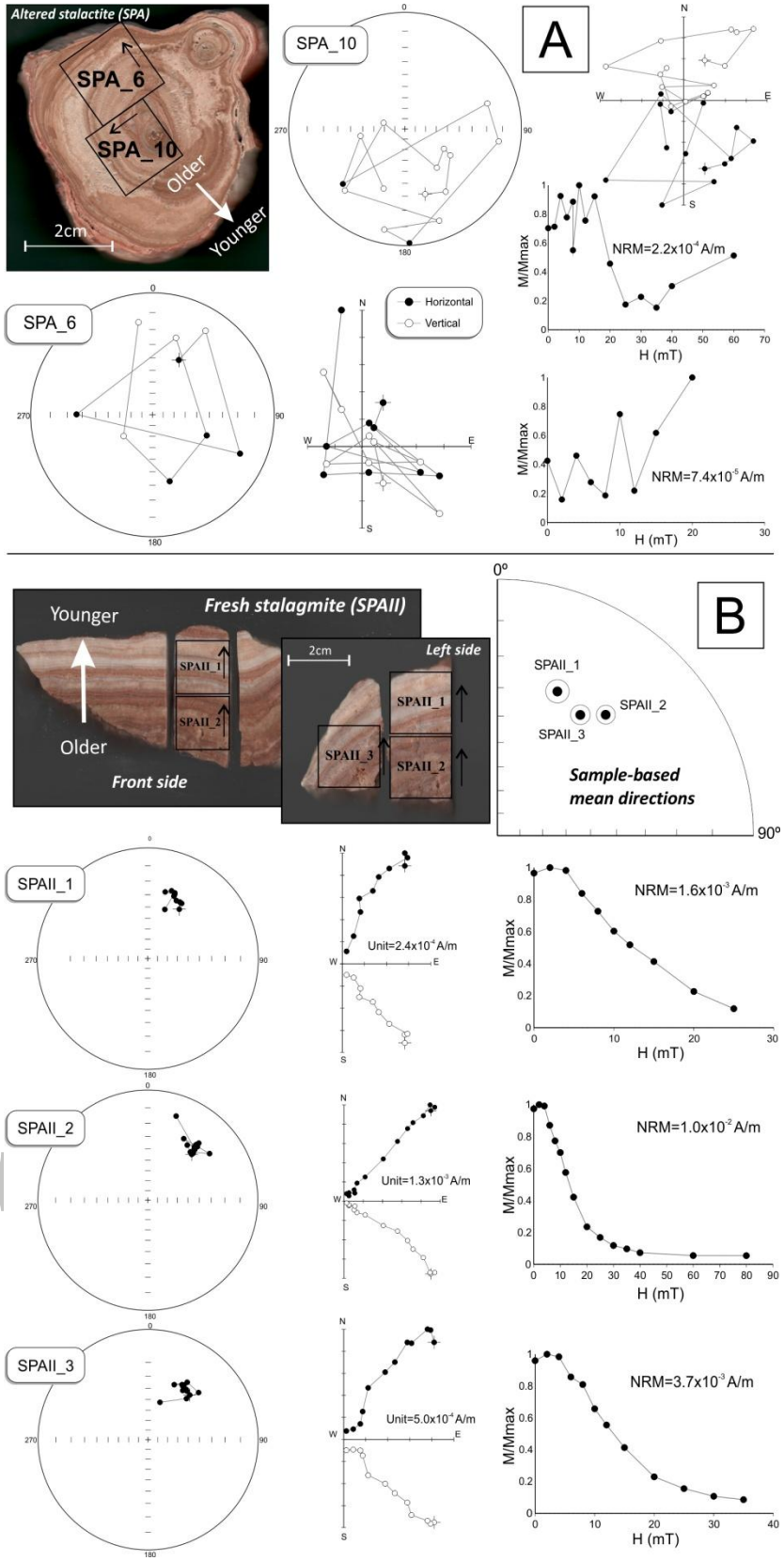

Figure 11. Stereographic and orthogonal projections and remanence intensities during Alternating Field (AF) cleaning of A) the weathered stalactite and B) the fresh stalagmite. The weathered stalactite presents very low remanence intensities varying from 10^{-5} to 10^{-4} A/m and an erratic behavior. The fresh stalagmite has remanence intensities superior to 10^{-3} A/m and exhibits reliable magnetic directions.

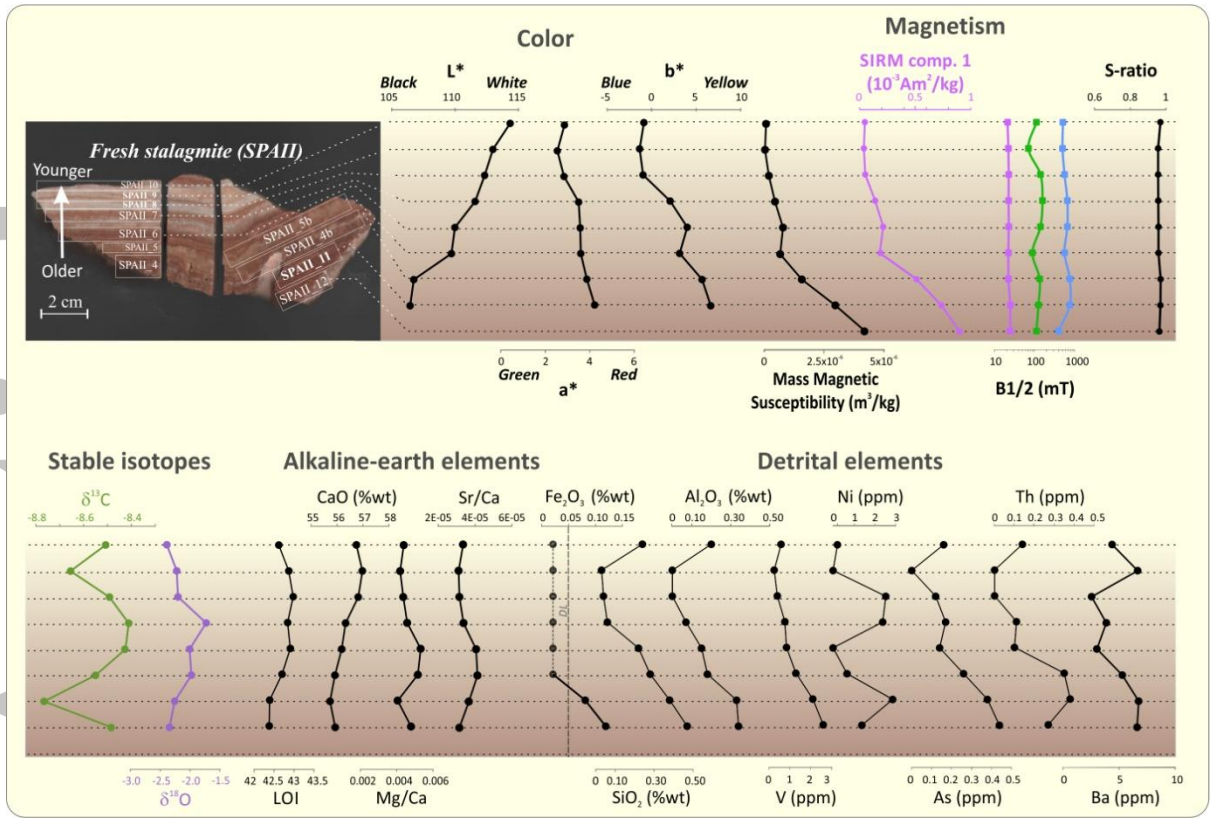

Figure 12. Visible Diffuse reflectance spectrophotometry (CIE L*, a* and b*), rock magnetic (Mass Magnetic Susceptibility, SIRM of comp. 1 (i.e. magnetite/maghemite), $B_{1/2}$ of comp. 1-2-3; S-Ratio), geochemical (selected major and trace elements) and carbon and oxygen isotopic composition of the fresh SPAII stalagmite. Color, concentration-dependent magnetic proxies (MS, SIRM comp. 1) and contents in detrital elements covary, while oxygen isotope composition and alkaline-earth element concentrations are independent.

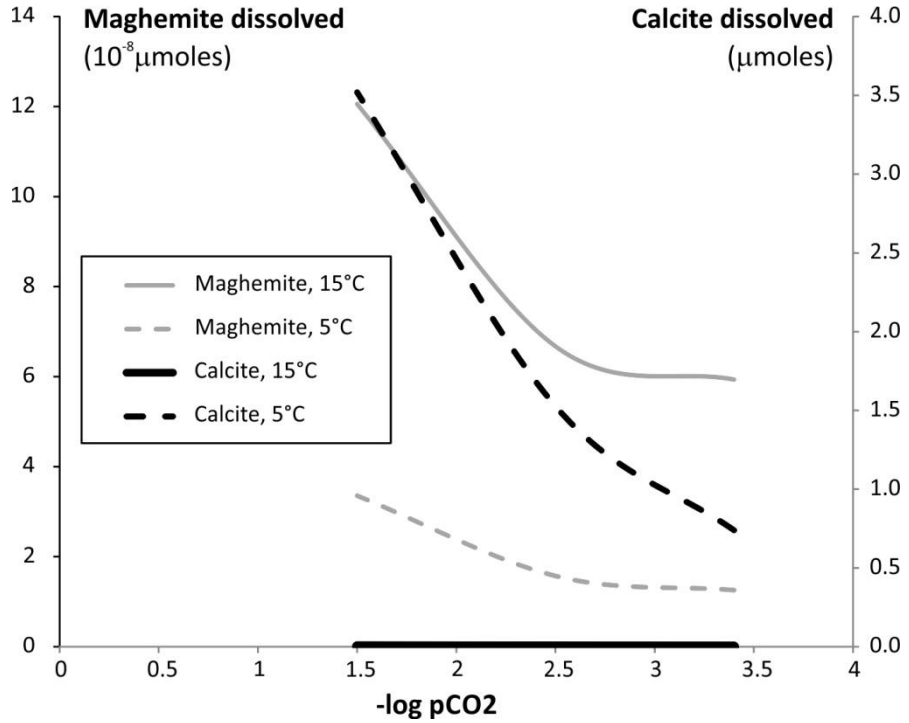

Figure 13. Number of dissolved moles of calcite (black line) and maghemite (grey line) needed to reach chemical equilibrium according to the CO_2 partial pressure expressed in -log units. Two temperatures are considered: 15°C (solid line) and 5ºC (dotted line).

Table 1: Carbon and oxygen stable isotope composition of the weathered and fresh speleothems under study (see also Fig. 5).

Sample	$\delta^{13}C_{VPDB}$	$\delta^{18}O_{VPDB}$
Weathered stalactite		
SPA1	-4.02	-2.53
SPA2	-4.15	-2.84
SPA3	-4.91	-1.49
SPA4	-2.93	-2.16
SPA5	-5.71	-2.61
Fresh stalagmite		
SPAII-10	-8.51	-2.39
SPAII-9	-8.65	-2.22
SPAII-8	-8.49	-2.20
SPAII-7	-8.41	-1.73
SPAII-6	-8.42	-2.01
SPAII-5B	-8.55	-1.98
SPAII-4B	-8.77	-2.26
SPAII-11	-8.48	-2.34

Table 2: Magnetic properties of the SPA and SPAII speleothems estimated by using mass specific magnetic susceptibility (Mass MS), Cisowski test (R and Hcr), modified Lowrie-Fuller test (SD- or MD-like response), ARM/SIRM ratio, hysteresis parameters (Mrs/Ms and Hcr/Hc) and unmixed IRM acquisition curves (CLG components; *Kruiver et al.* [2001]) (mass normalized saturation isothermal remanent magnetization=Mass SIRM, mean coercivity=$B_{1/2}$; Dispersion parameter=DP and percentage of remanence contribution). Note that SPAII samples are ordered following Figure 12.

Samples	**Mass MS (10^{-7} m^3/kg)**	**Cisowski (1981) test**		**Lowrie-Fuller Test (SD- or MD-like response)**	**Mrs/Ms**	**Hcr/Hc**	**CLG analysis**											
							S-ratio	**Comp. 1**				**Comp. 2**				**Comp. 3**			
		R	**Hcr (mT)**					**Mass SIRM (Am^2/kg)**	**$B_{1/2}$**	**DP**	**%**	**Mass SIRM (Am^2/kg)**	**$B_{1/2}$**	**DP**	**%**	**Mass SIRM (Am^2/kg)**	**$B_{1/2}$**	**DP**	**%**
SPA - weathered																			
SPA_2	-0.88	0.28	20	Mixed			0.89	1.25E-05	25	0.24	58	7.60E-06	89	0.25	35	1.34E-06	794	0.15	6
SPA_3	41.18	0.25	15	SD	0.11	3.93	0.94	1.05E-03	22	0.26	93	3.24E-05	166	0.25	3	4.32E-05	631	0.25	4
SPA_4	1.26	0.08	10	SD			0.91												
SPA_5	-1.14	0.26	17	Mixed			0.94	5.58E-06	22	0.26	54	4.41E-06	76	0.26	43	3.10E-07	447	0.20	3
SPA_7	-2.11	0.26	16	SD			0.93	3.16E-05	22	0.24	60	1.86E-05	76	0.26	35	2.26E-06	447	0.20	4

SPA_8	0.95	0.27	15.5	Mixed			0.93	9.39E-05	22	0.25	81	1.58E-05	100	0.30	14	5.55E-06	631	0.30	5
SPA_9	56.47	0.28	16	Mixed	0.13	3.98	0.92	2.35E-03	20	0.29	87	1.96E-04	100	0.25	7	1.57E-04	562	0.30	6
SPAII - fresh																			
SPAII_10	0.59	0.25	16	SD			0.94	4.71E-05	25	0.27	91	1.71E-06	112	0.24	3	2.86E-06	398	0.32	6
SPAII_9	0.14	0.24	16	SD			0.91	3.81E-05	25	0.28	91	1.14E-06	126	0.24	3	2.85E-06	759	0.26	7
SPAII_8	1.77	0.20	10	SD			0.91	5.00E-05	22	0.26	89	3.63E-06	135	0.32	6	2.79E-06	759	0.20	5
SPAII_7	4.34	0.26	15	SD			0.91	1.40E-04	22	0.25	89	7.35E-06	89	0.30	5	9.92E-06	562	0.28	6
SPAII_6	7.67	0.26	16	SD	0.09	4.92	0.92	2.13E-04	23	0.25	91	8.82E-06	141	0.30	4	1.10E-05	661	0.20	5
SPAII_5b	6.53	0.28	15	SD	0.07	5.42	0.92	1.81E-04	23	0.27	92	6.46E-06	158	0.25	3	9.50E-06	661	0.20	5
SPAII_5	12.24	0.26	15	SD			0.91	5.94E-04	25	0.28	91	2.46E-05	126	0.21	4	3.69E-05	525	0.20	6
SPAII_4	25.42	0.24	16	SD	0.10	3.48	0.96	8.11E-04	23	0.26	93	3.19E-05	100	0.25	4	2.56E-05	501	0.25	3
SPAII_4b	15.56	0.26	15	SD	0.14	2.92	0.94	5.11E-04	23	0.27	94	1.02E-05	141	0.20	2	2.25E-05	562	0.25	4
SPAII_11	29.59	0.26	15	SD	0.10	2.46	0.94	7.36E-04	22	0.26	92	2.66E-05	71	0.25	3	3.55E-05	501	0.25	4
SPAII_12	41.75	0.27	16	SD	0.09	4.99	0.93	9.00E-04	21	0.28	92	2.45E-05	112	0.28	3	4.91E-05	513	0.25	5

Table 3. Major elements content analyzed by X-ray fluorescence and minor elements analyzed by ICPMS of the fresh stalagmite (SPAII). $CaCO_3$ (%) is calculated by multiplying LOI values by 2.27 (the ratio of atomic masses of $CaCO_3$ and CO_2).

	SPA II 11	SPA II 4B	SPA II 5B	SPA II 6	SPA II 7	SPA II 8	SPA II 9	SPA II 10
Major elements (%wt)								
CaO	55.93	55.73	55.92	56.18	56.33	56.82	56.98	56.75
MgO	0.27	0.23	0.29	0.30	0.26	0.25	0.24	0.25
SiO_2	0.47	0.38	0.28	0.22	0.06	0.04	0.03	0.24
Al_2O_3	0.34	0.33	0.18	0.15	0.07	<0.10	<0.10	0.20
Fe_2O_3	0.12	0.08	<0.05	<0.05	<0.05	<0.05	<0.05	<0.05
TiO_2	<0.010	<0.010	<0.010	<0.010	<0.010	<0.010	<0.010	<0.010
MnO	<0.020	<0.020	<0.020	<0.020	<0.020	<0.020	<0.020	<0.020
K_2O	<0.10	<0.10	<0.10	<0.10	<0.10	<0.10	<0.10	<0.10
P_2O_5	<0.010	<0.010	<0.010	<0.010	<0.010	<0.010	<0.010	<0.010
Na_2O	0.04	0.04	0.03	0.03	0.03	0.03	0.04	0.04
LOI	42.62	42.87	42.98	42.84	42.91	42.70	42.39	42.38
CaCO3 (%)	96.7474	97.3149	97.5646	97.2468	97.4057	96.929	96.2253	96.2026
Trace elements (ppm)								
Sr	20.40	23.10	22.80	19.00	17.90	17.70	19.00	17.60
Be	< 0.1	< 0.1	< 0.1	< 0.1	< 0.1	< 0.1	< 0.1	< 0.1
V	2.10	1.29	0.84	0.76	0.40	0.25	0.58	2.60
Cr	< 2	< 2	< 2	< 2	< 2	< 2	< 2	< 2
Co	< 0.2	< 0.2	< 0.2	< 0.2	< 0.2	< 0.2	< 0.2	< 0.2
Ni	2.86	0.67	< 0.1	2.38	2.53	< 0.1	0.21	1.38
Cu	< 0.2	< 0.2	< 0.2	< 0.2	< 0.2	< 0.2	< 0.2	< 0.2
Zn	< 0.3	< 0.3	0.46	< 0.3	< 0.3	< 0.3	< 0.3	< 0.3
As	0.38	0.26	0.14	0.17	0.12	< 0.1	0.16	0.44
Mo	< 0.1	< 0.1	< 0.1	< 0.1	< 0.1	< 0.1	< 0.1	< 0.1
Ag	< 0.1	< 0.1	< 0.1	< 0.1	< 0.1	< 0.1	< 0.1	< 0.1
Cd	< 0.1	< 0.1	< 0.1	< 0.1	< 0.1	< 0.1	< 0.1	< 0.1
Ba	6.74	5.28	3.02	3.86	2.55	6.65	4.38	6.60
Pb	< 2	< 2	< 2	< 2	< 2	< 2	< 2	< 2
Th	0.38	0.35	0.10	0.11	< 0.1	< 0.1	0.14	0.27
U	< 0.1	< 0.1	< 0.1	< 0.1	< 0.1	< 0.1	< 0.1	< 0.1

Table 4. Correlation factors (R^2) between concentration-dependent magnetic proxies (MS and SIRM comp. 1), detrital input (Si content in %wt) and color (a* and b*).

	Si (%wt)	a*	b*
MS (m^3/kg)	R^2=0.711	R^2=0.757	R^2=0.772
SIRM comp. 1 (Am^2/kg)	R^2=0.7415	R^2=0.768	R^2=0.7415